Aeolus winds improve Arctic weather prediction

Chih Chun Gina Chou[1], Paul J. Kushner[1], and Zen Mariani[2]

[1]University of Toronto
[2]Environment and Climate Change Canada

March 15, 2024

Abstract

It has been proven that assimilating winds from the Aeolus global Doppler wind lidar would enhance the predictive skill of weather forecast models. In this study, we use a series of Observing System Experiments to examine how operational winds and Aeolus winds impact Environment and Climate Change Canada's global forecast system over the data-sparse Arctic region. Aeolus winds improve the tropospheric wind and temperature forecasts by about 0.7 to 0.9% of error reduction (a 15-20% effect compared to the impact of operational wind products), while having little impact on the specific humidity field. In particular, Aeolus winds have an impact on forecasts of strong wind days on the wind and temperature fields that is double the impact of the forecasts of less intense wind days and provides a disproportionate improvement to forecasts on these days compared to other operational wind measurements. These findings suggest significant potential for global doppler wind lidar observations to enhance severe-weather prediction in polar regions.

Aeolus winds improve Arctic weather prediction

C.-C. Chou[1], P. J. Kushner[1], and Z. Mariani[2]

[1]Department of Physics, University of Toronto, Toronto, M5S 1A7, Canada

[2]Meteorological Research Division, Environment and Climate Change Canada, Toronto, Canada

Corresponding author: Chih-Chun Chou (gina.chou@mail.utoronto.ca)

Key Points:

- Operational wind products are a key component of skillful numerical weather prediction in the Arctic.
- Augmenting operational winds with Aeolus winds could enhance the forecasts of winds and temperature fields by 14-18%.
- Aeolus wind improvements are most pronounced on strong wind days.

Abstract

It has been proven that assimilating winds from the Aeolus global Doppler wind lidar would enhance the predictive skill of weather forecast models. In this study, we use a series of Observing System Experiments to examine how operational winds and Aeolus winds impact Environment and Climate Change Canada's global forecast system over the data-sparse Arctic region. Aeolus winds improve the tropospheric wind and temperature forecasts by about 0.7 to 0.9% of error reduction (a 15-20% effect compared to the impact of operational wind products), while having little impact on the specific humidity field. In particular, Aeolus winds have an impact on forecasts of strong wind days on the wind and temperature fields that is double the impact of the forecasts of less intense wind days and provides a disproportionate improvement to forecasts on these days compared to other operational wind measurements. These findings suggest significant potential for global doppler wind lidar observations to enhance severe-weather prediction in polar regions.

Plain Language Summary

Wind observations are necessary to produce accurate weather forecasts. Aeolus is a new satellite that provides the first global wind profile measurements and it has a proven positive impact on forecasts. In this study, we investigate the impact of a large set of wind observations, including Aeolus winds, on Arctic weather forecasts using Canada's main forecast. We can calculate how these wind observations improve the forecast throughout the atmosphere, and find that Aeolus winds further improve the forecast in the lower atmosphere. Furthermore, our findings highlight the heightened significance of wind observations in ensuring precise forecasts of strong wind days. The difference is about double the improvement on the forecast of less intense wind days. This suggests that future doppler wind lidar programs following from Aeolus could significantly

benefit forecast skill in data-sparse regions like the Arctic and Antarctic, which are of growing societal, political, and economic interest.

1 Introduction

Arctic weather forecasts produced by operational numerical weather prediction (NWP) models present unique challenges (Bauer et al., 2016; Jung et al., 2016; Gascard et al., 2017). The Arctic presents unique logistical and environmental challenges that hinder real-time data collection and the maintenance of observation equipment (Randriamampianina et al., 2019; Lawrence et al., 2019; James et al., 2020; Joe et al., 2020; Chou et al., 2020). Furthermore, the Arctic's unique geography and rapidly changing climate contribute to unpredictable and extreme weather events (Cohen et al. 2014; Francis et al., 2017; Lawrence et al., 2019; Eikeland et al., 2022). Nevertheless, improving Arctic forecasts remains imperative for the safety of residents and travellers in the region. Furthermore with melting sea ice opening up new opportunities, the Arctic is gaining increasing importance for shipping and industry (Gascard et al., 2017; Eicken, 2013; Inoue et al., 2015). Finally, given implications of Arctic change for have sea level rise and altered weather patterns, accurate forecasts promises to improve our understanding of and ability to adapt to climate change (Cohen et al. 2014; Jung et al., 2014; Overland et al. 2015; Francis et al., 2017; Laroche and Poan, 2021).

An essential element in producing reliable forecasts is the initialization of NWP systems with precise and timely observational data (Inoue et al., 2015; Randriamampianina et al., 2021). These observations allow estimation of the present atmospheric state, enabling the NWP system to establish the initial conditions necessary for accurate forecasts. Wind is a fundamental component of atmospheric dynamics, influencing the movement of air masses, the formation and evolution of weather systems, and the transport and advection of heat, moisture, and other

atmospheric constituents (Baker et al., 1995; Graham et al., 2000; Naakka et al., 2019). Thus, wind observations play a pivotal role in NWP initialization, even after accounting for the balance that constrains winds given pressure and temperature measurements (Horányi et al., 2014; Naakka et al., 2019; James et al., 2020).

Observations of altitude-resolved winds are available through aircraft reports (AMDAR; Dai et al., 2014; James et al., 2020), radiosondes (Durre et al., 2018; Carminati et al., 2019; Rani et al., 2021), and wind profiling technologies (e.g., Doppler radar and lidar; Augustine and Zipser, 1987; Rogers et al., 1993; Liu et al., 2020). However, these observations are often sporadic and notably scarce, particularly over vast bodies of water like oceans and the polar regions. Passive space-based observations offer an alternative, with Atmospheric Motion Vectors (AMVs) estimating wind speed and direction based on cloud and water vapor movements (Velden et al., 2017; Mizyak et al., 2016). Additionally, space-based scatterometers provide surface winds over the ocean. Despite the advantages of AMVs in offering wind information across multiple tropospheric layers through multispectral water vapor remote sensing (Velden et al., 1997; Bormann and Thépaut, 2004; Le Marshall et al., 2008), they lack precision in altitude assignment and are limited to a few levels, hindering their representation of small-scale vertical wind profile structures. Conversely, spaceborne scatterometers focus only on near-surface ocean winds, with their accuracy highly dependent upon surface weather conditions (Chiara et al., 2017; Young et al., 2017).

The Aeolus mission, featuring the first spaceborne Doppler Wind Lidar (DWL), provides the first-ever global horizontal line-of-sight (HLOS) wind profile measurements. Studies have demonstrated that assimilating Aeolus HLOS winds into NWP systems significantly enhances forecast accuracy. Examples of operational forecast systems include those of ECMWF (Rennie

et al., 2021), NCMRWF (George et al., 2021), DWD (Martin et al., 2023), NOAA (Garrett et al., 2022), Météo-France (Pourret et al., 2022), and Environment and Climate Change Canada (ECCC; Laroche and St-James, 2022). Most of the improvements were found in the tropical troposphere to lower stratosphere. Notably, Aeolus winds have also demonstrated a beneficial impact on forecasts in data-sparse regions such as the Southern Hemisphere extra-tropics and the Arctic (Mile et al., 2022; Chou and Kushner, 2023; Zuo and Hasager, 2023).

Despite the good coverage that polar-orbiting satellites provide over the Arctic, more than 90% of the assimilated observations over the Arctic are microwave and infrarared radiances (Lawrence et al., 2019; Randriamampianina et al., 2021). As previously discussed, wind observations from conventional surface and aircraft measurements are extremely sparse in this region. Hence, it is important to assess the impact of existing wind observations and any additional wind observations over the Arctic to compare and determine their impact on NWP model performance over the Arctic.

In this study, we extend the work of Chou and Kushner (2023) and evaluate the impact of operational winds and Aeolus winds on the global forecast system of ECCC with a focus on the Arctic. Chou and Kushner (2023) used a series of Observing System Experiments (OSE), in which all operational winds or Aeolus winds are withheld in the assimilation and the forecasts are verified against the fifth-generation European Centre for Medium-Range Weather Forecasts (ECMWF) atmospheric reanalysis (ERA5, Hersbach et al., 2023). The integration of operational winds significantly enhanced tropospheric wind forecasts, particularly in tropical regions, resulting in an impressive 8% reduction in forecast error. Further augmenting these assimilations with Aeolus winds contributed an additional 0.7-0.9% improvement or about 10% of the impact of operational winds. Notably, Aeolus winds also proved beneficial in regions with limited data,

such as the Arctic and the extra-tropical Southern Hemisphere, demonstrating a reduction in forecast errors ranging from 0.5% to 0.9%. While operational winds contribute significantly to forecast improvement, unexpected occurrences such as the COVID-19 pandemic can disturb aircraft measurements, resulting in less precise forecasts during such periods (James et al., 2020). This circumstance, and the need to quantify Doppler wind lidar profiles' impact in isolation from other wind-observation systems, prompts the addition of this study's OSE labeled "CNTRL–wind+Aeolus" (refer to Section 2 for the experimental setup). This new OSE aims to specifically assess the isolated impact of Aeolus winds in the Arctic without the influence of other wind products.

Our investigation encompasses an assessment of the overall improvements in Arctic forecasts resulting from the assimilation of different sets of wind observations, as well as an exploration of the influence of wind observations on the forecasts related to enhanced kinetic energy and intense Integrated Vapor Transport (IVT). Henceforth, "disturbed" atmospheric state is used to describe days with strong winds or intense vapor transport. These two metrics were selected because of their large societal and economic impacts. Enhanced kinetic energy is commonly used as a severe-weather indicator, e.g. for severe storms, tornadoes, hurricanes, and typhoons (Palmén, 1958; DeMego and Bosart, 1982; Misra et al., 2013; Bass et al., 2017) and as an indirect indicator of extreme rainfall and flooding events (Brodie and Rosewell, 2007; Chang et al., 2017; Kim et al., 2022). Energetic systems can also transport substantial moisture from moisture sources, which can lead to weather-related water damage (Hills, 1978; Jiang, 2003; Chen et al., 2012; Martinez et al., 2019; Olaguera et al., 2021). Recent research suggests that ongoing climate changes are likely modifying IVT patterns, influencing the frequency and

intensity of future extreme weather events (Radic et al., 2015; Mattingly et al., 2016; Gershunov et al., 2017; Tan et al., 2019).

This paper is organized as follows: Section 2 outlines the experimental setup, including details on the ECCC global forecast system and OSE. In Section 3, we present impact scores by comparing forecasts to ERA5 and define strong wind and strong vapor transport events. Section 4 unveils our results on the impact of wind observations on forecasts over the Arctic and on atmospheric events in the region. Finally, Section 5 offers a discussion of the main conclusions derived from this study.

2 Experimental Setup

OSEs are used to evaluate and assess the impact of observational data on NWP models by adding or removing a set of observations that are assimilated into the NWP model (Bouttier and Kelly, 2001; Laroche and Poan, 2021; Laroche and St-James, 2022). In this study, we use an extension of the series of OSEs used in Chou and Kushner (2023) to examine the impact of the operational wind observations and of Aeolus HLOS winds on the Arctic forecasts of the Canadian Global Deterministic Prediction System (GDPS). The OSEs cover two seasons: from July 1 to September 30 2019 (summer 2019) and from December 1 2019 to March 31 2020 (winter 2020). The atmospheric component of the forecast system is the latest version of the operational Global Environmental Multiscale (GEM) model implemented at ECCC in 2019 (McTaggart-Cowan et al., 2019) and the ocean component of the forecast system is the NEMO ocean model (Smith et al., 2018). The model uses approximately 15 km horizontal grid spacing and 84 vertical levels. The data assimilation scheme is the operational four-dimensional ensemble-variational (4D-EnVar) (Buehner et al., 2015) system, with a 6-h assimilation window which includes over 13 million observations assimilated daily. Two forecasts were generated

daily (at 00 and 12 UTC). To minimize the computational cost, a coarser horizontal grid resolution of 39 km is employed and some aspects of the GEM physics are simplified. Implications of the use of this coarse resolution will be discussed in Section 5. Further details and justification on this simplified GDPS version are provided in Laroche and St-James (2022) and Chou and Kushner (2023). To examine the impact of wind observations, four experiments are carried out:

1. CNTRL, an experiment with all operational observations.
2. CNTRL–winds (i.e., "control-minus-winds"), an experiment with all operational observations except the operational wind observations. Operational winds include wind measurements from AMDAR, AMVs, radiosondes, surface stations, surface buoys, wind profilers, and scatterometry. This assesses the impact of all operational wind products on NWP skill.
3. CNTRL–wind+Aeolus (i.e., "control-minus-winds-plus-Aeolus"), an experiment with all operational observations and Aeolus HLOS winds (both Rayleigh-clear and Mie-cloudy winds) but without the operational wind observations. The winds used are from the second reprocessed product, the Level-2B11 product. This tests the impact of Aeolus winds in isolation from the other wind products and provides an assessment of NWP performance if traditional wind observations were halted (such as the reduction in AMDAR flights during Covid 19) but Aeolus was assimilated.
4. CNTRL+Aeolus (i.e., "control plus Aeolus"), an experiment that adds the Aeolus HLOS winds (both Rayleigh-clear and Mie-cloudy winds) to the CNTRL experiment. This tests the impact of Aeolus winds on top of the other wind products and provides an assessment of NWP performance if Aeolus winds were operationally assimilated.

Chou and Kushner (2023) used OSEs 1, 2, and 4. The current study is the first to use OSE 3 to test the effect of Aeolus wind impacts separately from other wind products.

To evaluate the impact of the wind observations, we compare the forecast root-mean-square error (RMSE) between the experiments. The mathematical expression of the forecast impact scores will be discussed in Section 3. Henceforth, the expression "impact of operational winds" (IOW) refers to the normalized change in the forecast scores from the CNTRL compared to the CNTRL–winds (i.e., error of CNTRL–winds minus error of CNTRL, which is therefore positive for improvement), the expression "impact of Aeolus winds" (IAW) refers to the change in the forecast scores from the CNTRL–winds+Aeolus compared to the CNTRL–winds (i.e., error of CNTRL–winds minus error of CNTRL–winds+Aeolus, which is therefore, again, positive for improvement), and the expression "impact of Aeolus on top of operational winds" (IAOW) refers to the change from the CNTRL+Aeolus compared to the CNTRL (i.e., error of CNTRL minus error of CNTRL+Aeolus, so, again, positive for improvement).

3 Method

We verify the forecasts from OSEs described in Section 2, against ERA5 from ECMWF (Hersbach et al., 2023). ERA5 is based on a four-dimensional variational (4DVar) data assimilation scheme using Cycle 41r2 of the Integrated Forecast System (IFS). We use the hourly winds, temperature, and specific humidity at 00 and 12 UTC. The data are gridded on a regular latitude-longitude grid of 0.25°, but linearly interpolated onto grid of 0.5° to match the coarser resolution of the OSEs, and only the OSEs' 16 pressure levels are selected (10, 20, 30, 50, 70, 100, 150, 200, 250, 300, 400, 500, 700, 850, 925, and 1000 hPa).

The impact of wind observations is defined as the normalized change (percentage change) in the forecast RMSE between the experiments over the Arctic. The steps to calculate the forecast RMSE are as follows:

1. Calculate the cosine-weighted mean-square-error (MSE) between the forecasts from OSEs and the verification field from ERA5, over the Arctic (70° to 90°N), for each forecast hour (two forecasts daily for a total of seven months). The MSE for a scalar field x (i.e., temperature, specific humidity, and IVT) is

$$MSE = \frac{\sum_i w_i \left(x_f - x_v\right)_i^2}{\sum_i w_i} \quad (1)$$

   and the MSE for a vector field $\vec{v}$ (i.e., vector wind and wind shear) is

$$MSE_{vector} = \frac{\sum_i w_i ||\vec{v}_f - \vec{v}_v||_i^2}{\sum_i w_i}. \quad (2)$$

   The index i indicates a grid point along a latitude band, the subscript f indicates the forecast, and the subscript v indicates the verification field. The weight $w_i = \cos\theta_i$, where θ_i is the latitude at location i.
2. The weighted MSEs are averaged over the seven months covering the available Aeolus observation products.
3. The square-root of the averaged weighted MSEs is the RMSE at each pressure level.
4. The normalized change in scores represents the percentage change of the RMSE between a pair of OSEs from Step 3.

5. The tropospheric impact score is the averaged scores from Step 4 from the four pressure levels: 850 hPa, 500 hPa, 250 hPa, and 100 hPa.

As introduced in Section 2, the impact of operational winds (IOW) is the percentage difference of forecast RMSE between CNTRL and CNTRL–winds; the impact of Aeolus winds (IAW) is the percentage difference of CNTRL–winds+Aeolus and CNTRL–winds; the impact of Aeolus on top of operational winds (IAOW) is the percentage difference of CNTRL+Aeolus and CNTRL.

Chou and Kushner (2023) show that adding Aeolus winds into data assimilation, which are the first global wind profile measurements, can improve the forecasts of the vertical structure of the wind field. We carry out this analysis in this study and will investigate the impact of wind observations on Arctic weather events on the tropospheric wind vector, temperature, wind shear (thermal-wind) vector (defined as the vector wind difference between 250 hPa and 850 hPa), specific humidity, and IVT. Analysis of specific humidity was included to help interpret the results of the IVT analysis.

For the second part of the paper (Section 4.2), we will discuss the impact of wind observations over the Arctic when the atmosphere is disturbed (i.e., strong kinetic energy or intense IVT). In preliminary work, we have investigated the impact of wind observations on localized events, such as strong wind events at radiosonde stations over the Arctic and forecasts along Aeolus swaths. This analysis is not shown in this study because, due to the short period of the Aeolus mission and the coarse resolution of the OSE forecasts, there were not many individual local events to average over, and we found that the OSEs had limited ability to resolve smaller-scale atmospheric features associated with severe Arctic weather such as polar lows. Instead, to investigate the impact of wind observations on predictability of extreme Arctic

weather events, we focus on days in which the atmosphere is strongly disturbed over the entire Arctic. In particular, we examine the impact of wind observations on the forecasts of "strong" 500-hPa Kinetic Energy (KE500) days vs. "normal" KE500 days, and of strong IVT days vs. normal IVT days over the Arctic. The KE500 ($m^2 s^{-2}$) is

$$KE500 = \frac{1}{2}(u^2 + v^2) \tag{3}$$

where u and v are the 500-hPa zonal and meridional wind components, respectively. The IVT ($kgm^{-1}s^{-1}$) is

$$IVT = \sqrt{\left(\frac{1}{g}\int_{1000}^{300} qudp\right)^2 + \left(\frac{1}{g}\int_{1000}^{300} qvdp\right)^2} \tag{4}$$

where g is the gravitational acceleration, q is the specific humidity, u and v are the zonal and meridional winds, and the product of the specific humidity and the winds is integrated over 1000, 925, 850, 700, 500, 400, and 300 hPa (Cordeira and Ralph, 2020; Reynolds et al., 2022).

We define the strong KE500 days and strong IVT days in a similar way. First, we define the threshold at each grid point as the 90th percentile of the local KE500 or the local IVT for the summer season and the winter season separately. We record the number of grid points poleward of 70°N that exceed this threshold and take the top 25% of this number for both seasons combined to get "strong weather-event days" with more disturbed atmospheric conditions. Trial and error suggests that this provides sufficient sampling to assess the impact of wind observations on the forecasts (Section 4.2).

4 Results

4.1 Impact of operational winds and Aeolus winds over the Arctic

Figure 1 shows the impact of operational winds (IOW), Aeolus winds (IAW), and Aeolus winds on top of operational winds (IAOW) on the tropospheric forecast RMSE over the Arctic. Note that the y-axis extends from -12 to 12% for the IOW (panel a) and from -4 to 4% for the IAW and IAOW (Figure 1b,c). As expected, operational wind observations notably enhance the forecasts of wind fields (vector wind and wind shear) and the temperature field, which provides a context for assessing the impacts of Aeolus (Chou and Kushner, 2023). Averaged scores for these three fields over five days demonstrate an improvement of approximately 5%. Replacing operational winds by Aeolus winds, IAW (Figure 1b), consistently delivers a positive impact of about 2%, constituting roughly 40% of the improvement achieved with all operational winds. It is noteworthy that Aeolus, despite being a single-satellite measurement system, contributes meaningfully to forecast enhancement.

Considering all operational winds, as reflected in the IAOW in Figure 1c, Aeolus winds further enhance the wind and temperature fields throughout the five-day forecast lead time by 0.7% and 0.9%, respectively, representing 14% to 18% of the overall improvement obtained with all operational winds. While this positive IAOW is relatively modest compared to improvements found by Aeolus for other models (e.g., Garrett et al., 2022; Rennie et al., 2021), it aligns with previous findings in OSEs conducted with the ECCC GDPS (Laroche and St-James, 2022; Chou and Kushner, 2023). The reasons for this modest impact are elaborated on in Chou and Kushner (2023). Despite the relatively small contribution, the impact of Aeolus winds on top of operational winds is noteworthy, particularly considering that Aeolus observations for this period constitute less than 1% of all operational wind observations. Notably, operational winds,

inclusive of measurements from various ground-based instruments, radiosondes, and satellites, account for roughly 10% of all operational observations over the Arctic in the ECCC GDPS. The lack of significance when assimilating Aeolus winds on top of operational winds might arise from the simplification and relatively coarse resolution of the ECCC model version used in this work to reduce computational cost, systematic model issues beyond this simplification, or assimilation system deficiencies, as discussed in Chou and Kushner (2023). Importantly, the IAW remains significant, reaching at least 90% confidence level, particularly in the wind fields for the first three days of the lead time.

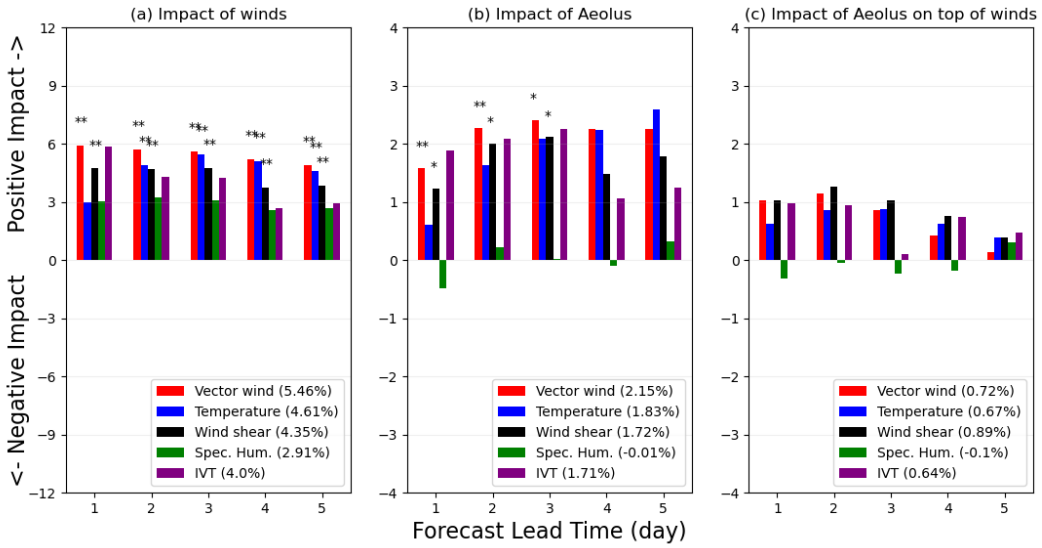

Figure 1: Normalized change in RMS forecast error between (a) CNTRL–winds and CNTRL (IOW), (b) CNTRL–winds and CNTRL–winds+Aeolus (IAW), and (c) CNTRL and CNTRL+Aeolus (IAOW), compared to ERA5 in the troposphere for vector wind (red), temperature (blue), wind shear (black), specific humidity (green), and integrated vapor transport (IVT) (purple) in the troposphere (850-100hPa layer) for 5-day forecasts over the Arctic. Positive impact means a reduction in the forecast error. The impacts that are significant at 95% confident level are marked with double asterisk (**) and impacts that are significant at 90% confident level are marked with single asterisk (*). The significance is tested using a t-test for the null hypothesis that the pair of experiments have identical cosine-

weighted RMSE from all four layers. The averaged impact over the five forecast lead time days is shown in the brackets.

Both operational winds and Aeolus winds show minimal to no impact on the specific humidity field, despite enhancements in other fields. The averaged IOW in Figure 1a over a five-day forecast lead time is approximately 3%, which is about half of the impact observed in the vector wind field. The IAW in Figure 1b and the IAOW in Figure 1c on the specific humidity field lack consistency throughout the forecast lead time. Consequently, the impact on the IVT, encompassing both wind and specific humidity information, falls between the impact on the wind fields and the specific humidity field. The averaged scores for the IVT are 4.0, 1.7, and 0.6% for the IOW, IAW, and IAOW, respectively.

Figure 2 provides a view of the spatial structure of the impact of wind observations on the vector wind field by breaking down the pressure-level and forecast lead time dependence (up to day 10). The tropospheric impacts observed in the first five days of the forecast lead time align with the findings depicted in Figure 1. Note that the color scale is compressed by factors of two when transitioning from the IOW in Figure 2a to the IAW in Figure 2b, and to the IAOW in Figure 2c. This demonstrates, consistently with Figure 1, that IAW contributes to about half of the improvement obtained by all operational winds. In the case of tropospheric IAOW, the enhancements from Aeolus winds on top of operational winds exceed 25% of the improvement obtained with all operational winds in short-range forecasts and are slightly less than 20% in short- to medium-range forecasts.

Conversely, Figure 2 reveals a degradation in forecast skills when assimilating Aeolus in the stratosphere. As previously discussed in Chou and Kushner (2023), this issue may arise from

the simplification of the ECCC model version used to reduce computational costs, systematic model issues beyond this simplification, or deficiencies in the assimilation system.

Overall, Figure 2 underscores the potential of Aeolus to enhance medium- to long-range forecasts, particularly in the upper atmosphere beyond day 4. The IAW accounts for more than 50% of the improvements from operational winds, and more than 25% for the IAOW. This stratospheric improvement in long-range forecasts over the Arctic is primarily attributed to the signal during the winter season, characterized by an anomalously strong Arctic stratospheric polar vortex in 2019-2020 (Chou and Kushner, 2023; Lawrence et al., 2020).

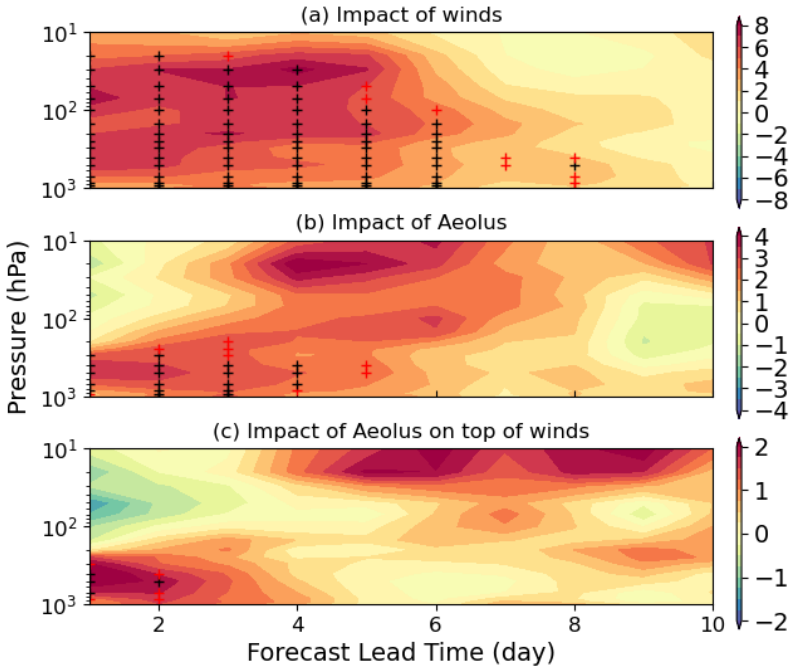

Figure 2: Normalized change in RMS forecast error as a function of pressure level between (a) CNTRL–winds and CNTRL, (b) CNTRL–winds and CNTRL–winds+Aeolus, and (c) CNTRL and CNTRL+Aeolus, for wind vector for 10-day forecasts over the Arctic. Positive impact means a reduction in the forecast error. The impacts that are significant at 95% confident level are marked with black plus sign and impacts that are significant at 90% confident

level are marked with red plus sign. The scores with respect to ERA5 data are interpolated onto the 16 pressure levels of the OSEs.

Despite previous challenges in attributing improvements in the Arctic forecast to localized regions, some regional insight can be gained by including all forecasts and dividing the Arctic into quadrants. We repeat the pan-Arctic analysis for four Arctic quadrants and investigate the IOW, IAW, and IAOW on the wind and temperature fields over each quadrant (SFigures 1 to 3 respectively). This shows that over the Arctic, Russian-Pacific-Northern Canada sector forecasts (90°E –180°E and 180°E–270°E) are most improved and sensitive to the wind observations; the IOW on the vector wind field are 5.7% and 6.7%, compared to 4.6% and 5.0% over the other two quadrants and similar results are found when Aeolus winds are assimilated. The IAW and IAOW on the vector wind field are around 2.7 and 0.8% respectively over the quadrants between 90° and 270°E, which are about 40 and 13% of the IOW, but the impacts are only around 1.6 and 0.6% over the other two quadrants, which are 33 and 12% compared to IOW. The reason why this region's forecasts are more sensitive to wind observations remains unclear, but it is consistent when different sets of wind observations are assimilated into the forecast model. There are many aspects that can lead to this difference; for example, the proportion of land, ocean, and snow/ice, number of observations over the region, and the physics used for the region in the model. However, such investigations are beyond the scope of this paper.

4.2 Impact of wind observations on strong wind and vapor transport events over the Arctic

We are interested in whether wind observations would improve the forecasts of severe weather events and how much in advance the forecasts would show an improvement. More

specifically, this subsection presents the impact of wind observations on strong wind events and water vapor transport events over the Arctic. The proportions of the Arctic that exceed the KE500 and IVT thresholds (90^{th} percentile of the field of the season) are recorded at each forecast hour and the time-series of this spatial coverage ratio are shown in Figures 3 and 4, respectively. The days that are defined as more energized or in a more disturbed atmospheric state are the top 25% (red dots) of this spatial coverage ratio during the entire period of analysis. For these events at and above the 75^{th} percentile, the forecasts that are defined as strong KE500 occur when at least 13% of the Arctic points exceed the thresholds of the field, and the forecasts that are defined as strong IVT occur when at least 12% of the Arctic exceed the threshold of the field. Strong KE500 forecasts do not necessarily overlap with the forecasts that have strong IVT. For example, before mid-July 2019, there are around eight forecasts that experienced strong IVT, but none of the forecasts during this period are defined as strong KE500 forecasts. Also, at the end of December 2019 and in early January 2020, most of the forecasts show an energetic, strong KE500, atmosphere, but the IVT over the Arctic during this period is relatively weak. By grouping the forecasts using the top 25%, we get sufficient forecasts (around 100 forecasts) to compare and to investigate the impact of wind observations on disturbed atmospheric states.

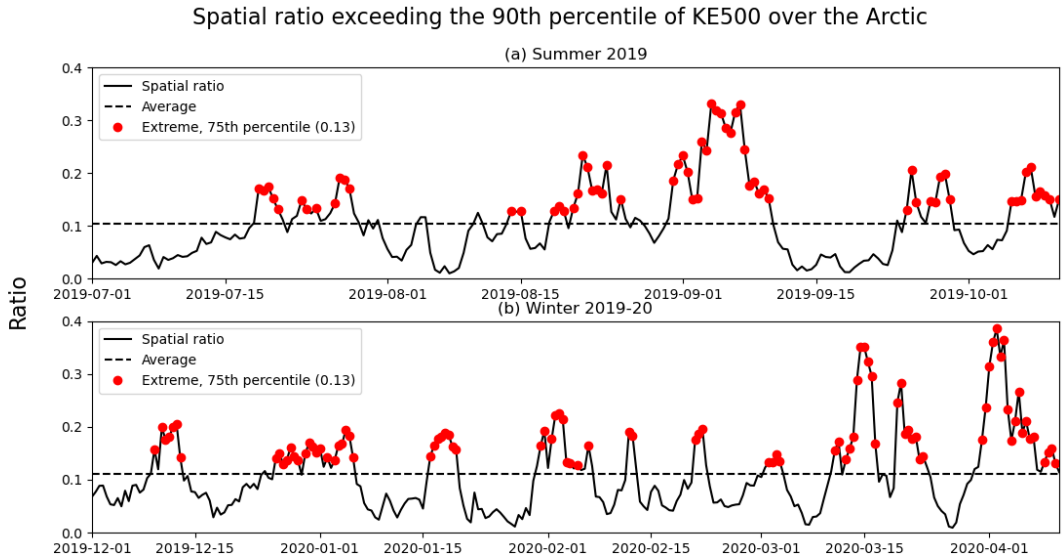

369

370 Figure 3: The time-series (solid black line) during (a) summer 2019 and (b) winter 2019-20 of the spatial coverage
371 ratio that exceeds the 90th percentile of the 500-hPa Kinetic Energy of the season over the Arctic. The time-averaged
372 of the spatial ratio of the season is shown as the dashed black line. The strong KE500 days (red dots) are defined as
373 when the spatial ratio exceeds the 75th percentile of the two seasons combined. The threshold of the spatial ratio (the
374 75th percentile) is indicated in the legend for the extreme days.

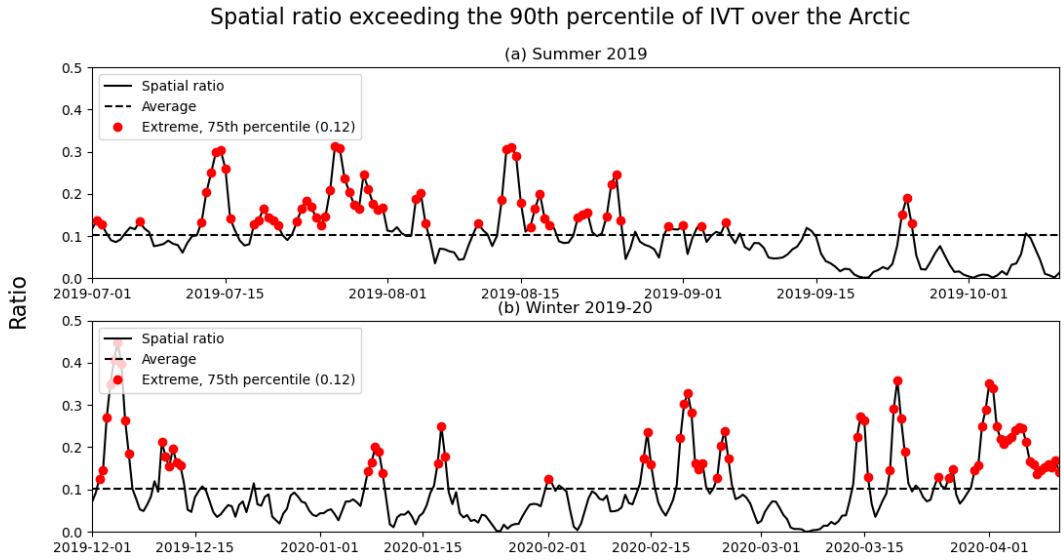

375

Figure 4: Similar to Figure 3, but for the spatial coverage ratio that exceeds the 90th percentile of the IVT over the Arctic.

We use the same approach, outlined in Section 3, to find the normalized change in the forecast RMSE between a pair of experiments, but we composite tropospheric forecast skill impacts conditioned on strong (Figure 5a,b,c) and normal (Figure 5d,e,f) Arctic KE500, and on strong (Figure 6a,b,c) and normal (Figure 6d,e,f) Arctic IVT. Note that the x-axis is showing the forecast "ahead" time, instead of the forecast lead time as shown in Figures 1 and 2. The forecast ahead time represents the number of days prior to the identified disturbed atmospheric day, as measured with KE500 or IVT. For instance, if there is a strong wind event on July 15th, then the scores show the impact of wind observations on forecasts of July 15th that were made prior to the event. If the score for forecasts of two-day ahead time is 2%, then it means that the forecast RMSE with two-day lead time that was made on July 13th is reduced by 2% when wind observations are assimilated.

The wind observations consistently provide more positive impact on forecasts of strong KE500 on wind and temperature fields. For example, the IOW on forecasts of normal KE500 is around 4.6% and it increases to around 5.8% when conditioned on forecasts of strong KE500. Consistent findings are noted with the assimilation of Aeolus winds. The impact scores show an increase from 1.8 to 2.4% when operational winds are replaced by Aeolus winds, when conditioned on normal (Figure 5e) and strong (Figure 5b) KE500 days. Specifically, the IAOW for forecasts of strong KE500 is nearly triple the impact scores observed when conditioned on normal KE500 days. The averaged scores over the five forecast lead times rise from 0.6 to 1.5%.

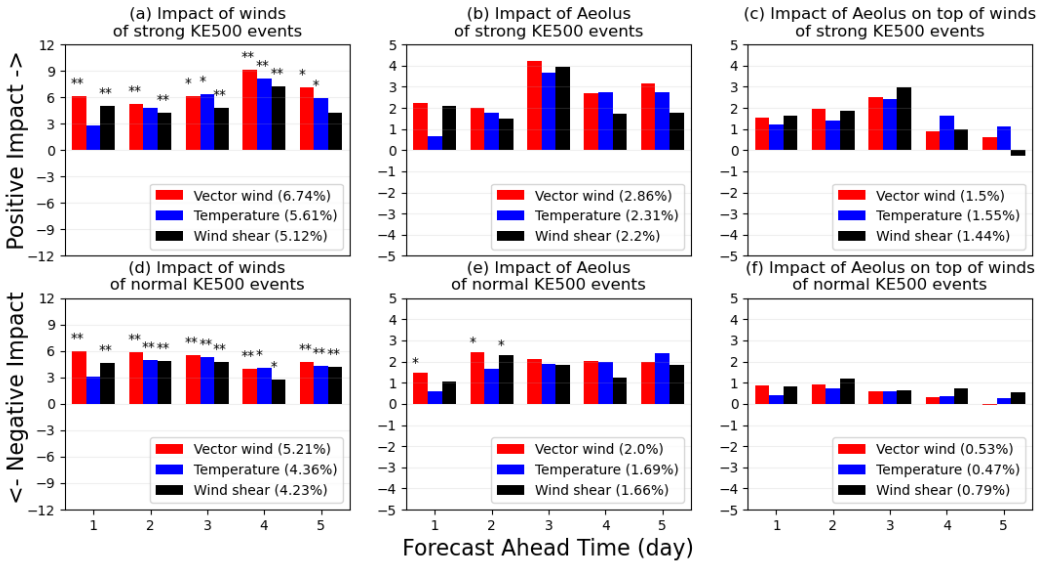

397

398 Figure 5: Normalized change in RMS forecast error for IOW (left column), IAW (middle column), and IAOW (right
399 column) for vector winds, temperature and wind shear, as a function of "Forecast Ahead Time" (see text), for strong
400 KE500 forecasts only (top row) and normal KE500 forecasts only (bottom row). Note that the scale of the y-axis
401 extends from -5 to 5% for panels b, c, e, and f. Significance testing as in Figure 1. Strong KE500 events are defined
402 in Figure 3; the remaining KE500 events are identified as "normal".

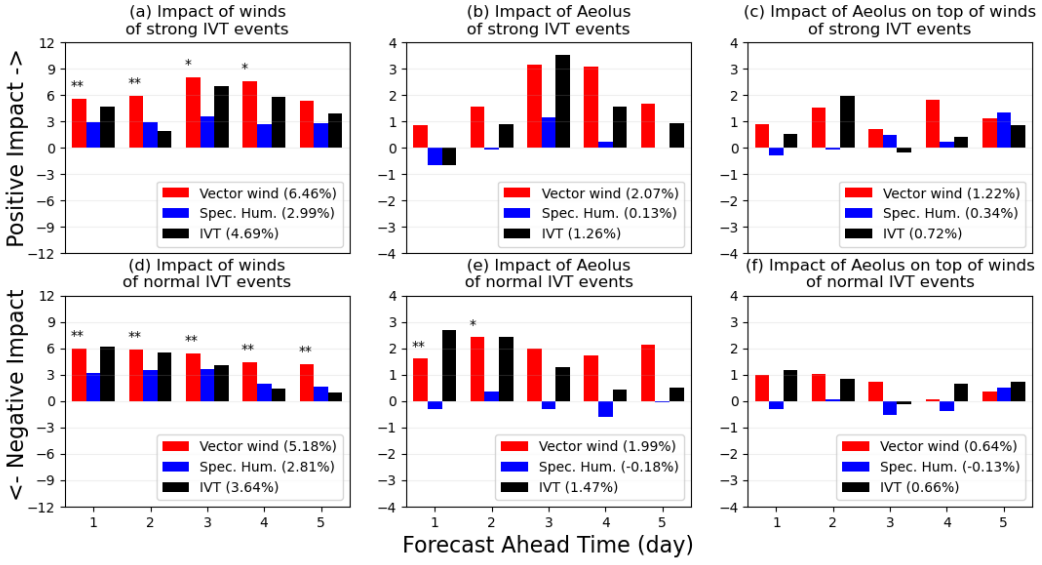

403

Figure 6: Similar to Figure 5, but for vector winds, specific humidity, and IVT, for strong and normal IVT events defined in Figure 4.

Greater impacts are also seen when conditioned on forecasts of strong IVT (Figure 6a,b,c) compared to forecasts of normal IVT (Figure 6d,e,f). The IOW on the wind field increases by approximately 1.3% when conditioned on strong IVT and by 1.0% for the IVT field. Conversely, the averaged IAW over five days shows little to no difference when conditioned on forecasts of strong IVT days (Figure 6b,e). The impact scores averaged over the five forecast lead times on the wind and IVT fields exhibit no more than a 0.2% difference. If Aeolus winds are assimilated on top of operational winds, the IAOW would approximately double the impact scores for the wind field when conditioned on forecasts of strong IVT (Figure 6c). Generally, Aeolus winds (Figure 6b,c,e,f) demonstrate little to no consistent impact on the specific humidity field.

The results from Figure 5 encourage us to investigate the profiles of impact of wind observations conditioned on strong (Figure 7a,c,e) and normal (Figure 7b,d,f) Arctic KE500 with a longer forecast ahead time. Profiles of impact conditioned on strong and normal Arctic IVT are shown in the supplementary information (SFigure 6). The operational winds reduce the forecast RMSE by more than 8% throughout the atmosphere with 3 to 5 days of lead time before strong KE500 days (Figure 7a), whereas they only reduce the forecast RMSE by about 4% for normal KE500 (Figure 7b). When operational winds are replaced by Aeolus winds, the IAW on forecasts of strong KE500 with a lead time of 3 to 5 days (Figure 7c) accounts for approximately 50% of the improvement obtained with all operational winds. Consistently with our findings above, the IAW is about 40% of the IOW and the IAW impact on strong KE500 days is greater than on normal KE500 days (Figures 7c-d), and IAOW is about 25% of the IOW, with extended lower

tropospheric impacts four or more days ahead being evident for the strong KE500 days, which is not as evident for the normal KE500 days (Figures 7e-f).

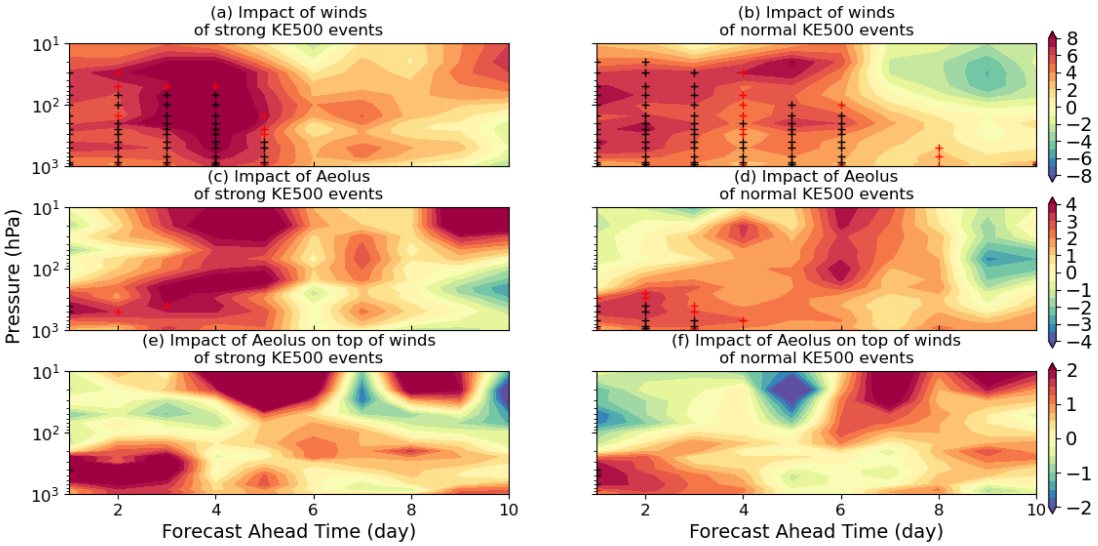

Figure 7: Normalized change in RMS forecast error as a function of pressure level for IOW (top row), IAW (middle row) and IAOW (bottom row), for wind vector errors up to 10 forecast days ahead. Positive impact means a reduction in the forecast error. The left column shows the impact of the added wind observations respectively of the strong KE500 days only defined in Figure 3 and column two shows the impact of the non-strong KE500 days only. Significance testing as in Figure 2.

5 Conclusions

The Arctic has fewer weather observation stations and limited data sources due to its low population density, limited accessibility, and harsh environment. However, the Arctic's distinctive geography, increasing economic activity, global geopolitical importance, and rapidly evolving climate changes necessitate advances in weather modeling and forecasting. Precise weather predictions in the Arctic are crucial for the safety of individuals and navigation in the area, and a deeper comprehension of Arctic weather has the potential to improve global climate models.

To better understand the role of wind observations in the weather forecasts over the Arctic, we have assessed the impact of operational winds (IOW), Aeolus winds (IAW), and Aeolus winds on top of operational winds (IAOW) on the ECCC global forecast system over the Arctic during July to September 2019 and December 2019 to March 2020. The analysis covers both the difference between disturbed atmospheric conditions (high versus normal KE500 and IVT days) and surveys different Arctic sectors for improvements. This extends Chou and Kushner (2023) who examined the general scale dependence and global distribution of IOW and IAOW. The IAOW has been enabled by the new experiment without the operational winds but with the Aeolus winds (CNTRL–winds+Aeolus), which allows us to study the impact of Aeolus winds as if it were, hypothetically, the only source of wind observations.

As anticipated, operational winds significantly enhance Arctic forecasts, reducing forecast RMSE by approximately 5%, particularly in the wind and temperature fields. This improvement is even greater for disturbed atmospheric conditions, as measured by high KE500 and IVT values. This highlights how wind observations become even more important during extreme atmospheric states where simple dynamical balances that couple mass and circulation break down. Despite Aeolus winds representing less than 1% of operational wind observations, substituting operational winds with Aeolus winds in the assimilation process results in an observed 2% reduction in errors, equivalent to approximately 40% of the improvement achieved by operational winds. This improvement extends to the additional forecast improvements seen on strong KE500 and IVT days. Thus, despite being derived from a single satellite, Aeolus winds can match nearly half of the forecast enhancement realized by operational winds, which incorporate wind measurements from multiple ground-based instruments, radiosondes, and satellites. This suggests that Doppler wind lidar systems have the potential to strongly

complement conventional wind observations. This was already seen when Aeolus data was shown, during the COVID-19 pandemic, to be capable of compensating for the disruption of AMDAR aircraft wind measurements and consequent forecast degradation (James et al., 2020). Altogether, assimilating Aeolus winds on top of operational winds (IAOW) yields an additional 0.8% reduction in errors, constituting around 16% of the overall improvement obtained with all operational winds.

While wind observations exhibit positive outcomes for mass-related fields like temperature, operational winds only contribute approximately half of the impact on the specific humidity field compared to the temperature field. Additionally, both the IAW and IAOW show little to no influence on the specific humidity field over the Arctic. This suggests that wind observations have limited efficacy in improving the specific humidity field.

As noted, Aeolus not only improves overall forecasts over the Arctic but also improves predictions for specific days characterized by strong winds and enhanced water vapor transport, which are associated with extreme weather events. In particular, the IAOW further reveals a two to threefold increase in impact scores (ranging from 0.5 to 1.5% for strong KE500 and 0.6 to 1.2% for intense IVT) on the wind field when forecasts are conditioned on a disturbed atmosphere, as opposed to normal days. While these results are found consistently in our diagnostics, their statistical significance is marginal and, we expect, will depend strongly on the smaller scale phenomena associated with extreme wind and IVT events. We thus strongly recommend conducting longer periods of OSEs at a higher resolution or with the use of a limited area regional forecast model.

The results also provide a compelling rationale for ECCC and other modelling centres to consider the operational assimilation of Aeolus winds. In particular, results have demonstrated

enhancements in forecast skill over data-sparse regions such as the Canadian Arctic, and for forecasts of intense wind events linked to extreme weather patterns, which can have large health, societal, and economic impacts. Notably, several European weather forecast centers, including ECMWF, DWD, Météo-France, and UK Met Office, have already embraced assimilation of Aeolus (Rennie et al., 2021; Pourret et al., 2022; Kiriakidis et al., 2023). Therefore, we recommend that weather forecast centers consider assimilating global wind profile measurements from the potential Aeolus follow-on mission, Aeolus-2, scheduled for launch in 2030 (Heliere et al., 2023).

Acknowledgments

We thank Stéphane Laroche from ECCC for the Observing System Experiments, and the ECMWF for the ERA5 data. We were supported by the Canadian Space Agency's Earth System Science Data Analysis program.

Data availability

The OSEs' MSE verified against ERA5 can be downloaded from the Borealis (https://doi.org/10.5683/SP3/C0XY1B). The ERA5 data can be downloaded from the Copernicus Climate Change Service (C3S) Climate Date Store (https://doi.org/10.24381/cds.bd0915c6, Hersbach et al., 2023).

References

Augustine, J. A., & Zipser, E. J. (1987). The Use of Wind Profilers in a Mesoscale Experiment. *Bulletin of the American Meteorological Society*, *68*(1), 4-17. https://doi.org/10.1175/1520-0477(1987)068<0004:TUOWPI>2.0.CO;2

Baker, W. E., Emmitt, G. D., Robertson, F., Atlas, R. M., Molinari, J. E., Bowdle, D. A., Paegle, J., Hardesty, R. M., Menzies, R. T., Krishnamurti, T. N., Brown, R. A., Post, M. J., Anderson, J. R., Lorenc, A. C., & McElroy, J. (1995). Lidar-Measured Winds from Space: A Key Component for Weather and Climate Prediction. *Bulletin of the American Meteorological Society*, *76*(6), 869-888. https://doi.org/10.1175/1520-0477(1995)076<0869:LMWFSA>2.0.CO;2

Bass, B., Irza, J.N., Proft, J. *et al.* (2017). Fidelity of the integrated kinetic energy factor as an indicator of storm surge impacts. *Nat Hazards* **85**, 575–595. https://doi.org/10.1007/s11069-016-2587-3

Bauer, P., Magnusson, L., Thépaut, J.-N. and Hamill, T.M. (2016), Aspects of ECMWF model performance in polar areas. Q.J.R. Meteorol. Soc., 142: 583-596. https://doi.org/10.1002/qj.2449

Bormann, N., & Thépaut, J.-N. (2004). Impact of MODIS polar winds in ECMWF's 4D-VAR data assimilation system. *Monthly Weather Review*, 132, 929–940.

Bouttier, F. and Kelly, G. (2001), Observing-system experiments in the ECMWF 4D-Var data assimilation system. *Quarterly Journal of the Royal Meteorological Society*, 127: 1469-1488. https://doi.org/10.1002/qj.49712757419

Brodie, I. and Rosewell, C. (2007). Theoretical relationships between rainfall intensity and kinetic energy variants associated with stormwater particle washoff. *Journal of Hydrology*, Volume 340, Issues 1–2, 2007, Pages 40-47, ISSN 0022-1694. https://doi.org/10.1016/j.jhydrol.2007.03.019

Buehner, M., McTaggart-Cowan, R., Beaulne, A., Charette, C., Garand, L., Heilliette, S., Lapalme, E., Laroche, S., Macpherson, S. R., Morneau, J., & Zadra, A. (2015). Implementation of Deterministic Weather Forecasting Systems Based on Ensemble–Variational Data Assimilation at Environment Canada. Part I: The Global System. *Monthly Weather Review*, *143*(7), 2532-2559. https://doi.org/10.1175/MWR-D-14-00354.1

Carminati, F., A. Migliorini, S., Ingleby, B., Bell, W., Lawrence, H., Newman, S., Hocking, J., & Smith, A. (2019). Using reference radiosondes to characterise NWP model uncertainty for improved satellite calibration and validation. *Atmospheric Measurement Techniques*, *12*(1), 83-106.

Chang, J.-M., Chen, H., Jou, J.-D., Tsou, N.-C., and Lin, G.-W. (2017). Characteristics of rainfall intensity, duration, and kinetic energy for landslide triggering in Taiwan. *Engineering Geology*, Volume 231, Pages 81-87, ISSN 0013-7952. https://doi.org/10.1016/j.enggeo.2017.10.006

Chen, C.-S., Lin, Y.-L., Zeng, H.-T., Chen, C.-Y., and Liu, C.-L. (2012). Orographic effects on heavy rainfall events over northeastern Taiwan during the northeasterly monsoon season. *Atmospheric Research*, Volume 122, 2013, Pages 310-335, ISSN 0169-8095. https://doi.org/10.1016/j.atmosres.2012.10.008

Chiara, G. D., Bonavita, M., & English, S. J. (2017). Improving the Assimilation of Scatterometer Wind Observations in Global NWP. IEEE Journal of Selected Topics in Applied Earth Observations and Remote Sensing, 10(5), 2415-2423. https://doi.org/10.1109/JSTARS.2017.2691011

Chou, C.-C. & Kushner, P.J. (2023) Scale-dependent impact of *Aeolus* winds on a global forecast system. *Quarterly Journal of the Royal Meteorological Society*, 1–15. https://doi.org/10.1002/qj.4601

Chou, C.-C., Kushner, P. J., Laroche, S., Mariani, Z., Rodriguez, P., Melo, S., and Fletcher, C. G.: Validation of the Aeolus Level-2B wind product over Northern Canada and the Arctic, Atmos. Meas. Tech., 15, 4443–4461, https://doi.org/10.5194/amt-15-4443-2022

Cohen, J., Screen, J., Furtado, J. *et al.* (2014). Recent Arctic amplification and extreme mid-latitude weather. *Nature Geosci* **7**, 627–637. https://doi.org/10.1038/ngeo2234

Cordeira, J. M., & Ralph, F. M. (2021). A Summary of GFS Ensemble Integrated Water Vapor Transport Forecasts and Skill along the U.S. West Coast during Water Years 2017–20. *Weather and Forecasting*, *36*(2), 361-377. https://doi.org/10.1175/WAF-D-20-0121.1

Dai, C., Wang, Q., Kalogiros, J. A., Lenschow, D. H., Gao, Z., & Zhou, M. (2014). Determining boundary-layer height from aircraft measurements. *Boundary-layer meteorology*, *152*, 277-302.

DiMego, G. J., & Bosart, L. F. (1982). The Transformation of Tropical Storm Agnes into an Extratropical Cyclone. Part II: Moisture, Vorticity and Kinetic Energy Budgets. *Monthly*

574 *Weather Review*, *110*(5), 412-433. https://doi.org/10.1175/1520-
575 0493(1982)110<0412:TTOTSA>2.0.CO;2

576 Durre, I., Yin, X., Vose, R. S., Applequist, S., & Arnfield, J. (2018). Enhancing the Data
577 Coverage in the Integrated Global Radiosonde Archive. *Journal of Atmospheric and*
578 *Oceanic Technology*, *35*(9), 1753-1770. https://doi.org/10.1175/JTECH-D-17-0223.1

579 Eicken, H. (2013). Arctic sea ice needs better forecasts. *Nature*, *497*(7450), 431-433.

580 Eikeland, O. F., Hovem, F. D., Olsen, T. E., Chiesa, M., Bianchi. F. M. (2022). Probabilistic
581 forecasts of wind power generation in regions with complex topography using deep
582 learning methods: An Arctic case. *Energy Conversion and Management: X*, Volume 15,
583 2022, 100239, ISSN 2590-1745. https://doi.org/10.1016/j.ecmx.2022.100239

584 Francis, J.A., Vavrus, S.J. and Cohen, J. (2017), Amplified Arctic warming and mid-latitude
585 weather: new perspectives on emerging connections. *WIREs Clim Change*, 8: e474.
586 https://doi.org/10.1002/wcc.474

587 Garrett, K., Liu, H., Ide, K., Hoffman, R.N. & Lukens, K.E. (2022). Optimization and impact
588 assessment of Aeolus HLOS wind assimilation in NOAA's global forecast
589 system. *Quarterly Journal of the Royal Meteorological Society*, 148(747), 2703–2716.
590 https://doi.org/10.1002/qj.4331

591 Gascard, JC., Riemann-Campe, K., Gerdes, R. *et al.* (2017). Future sea ice conditions and
592 weather forecasts in the Arctic: Implications for Arctic shipping. *Ambio* **46** (Suppl 3),
593 355–367. https://doi.org/10.1007/s13280-017-0951-5

594 George, G., Halloran, G., Kumar, S., Rani, S. I., Bushair, M.T., Jangid, B. P., George, J. P., and
595 Maycock, A. (2021). Impact of Aeolus Horizontal Line of Sight Wind Observations in a

Global NWP System" *Atmospheric Research* 261 (October): 105742. https://doi.org/10.1016/j.atmosres.2021.105742

Gershunov, A., Shulgina, T., Ralph, F. M., Lavers, D. A., and Rutz, J. J. (2017), Assessing the climate-scale variability of atmospheric rivers affecting western North America, *Geophyical Research Letter.*, 44, 7900–7908, doi:10.1002/2017GL074175.

Graham, R.J., Anderson, S.R. and Bader, M.J. (2000), The relative utility of current observation systems to global-scale NWP forecasts. *Quarterly Journal of the Royal Meteorological Society*, 126: 2435-2460. https://doi.org/10.1002/qj.49712656805

Heliere, A., Wernham, D., Mason, G., De Villele, G., Corselle, B., Lecrenier, O., Belhadj, T., Bravetti, P., Arnaud, S., Bon, D., Lingot, P., Foulon, R., Marchais, D., Olivier, M., D'Ottavi, A., Verzegnassi, F., Mondello, A., Coppola, F., Landi, G., Hoffmann, H.-D., Esser, D., Prieto, L.P., Wührer, C., Rivers, C., Bell, R. (2023). Status of Aeolus-2 mission pre-development activities. Proc. SPIE 12777, *International Conference on Space Optics — ICSO 2022*, 1277709. https://doi.org/10.1117/12.2688794

Hersbach, H., Bell, B., Berrisford, P., Biavati, G., Horányi, A., Muñoz Sabater, J., Nicolas, J., Peubey, C., Radu, R., Rozum, I., Schepers, D., Simmons, A., Soci, C., Dee, D., Thépaut, J-N. (2023). ERA5 hourly data on pressure levels from 1940 to present. Copernicus Climate Change Service (C3S) Climate Data Store (CDS). https://doi.org/10.24381/cds.bd0915c6

Hills, R. C. (1979). The Structure of the Inter-Tropical Convergence Zone in Equatorial Africa and Its Relationship to East African Rainfall. *Transactions of the Institute of British Geographers*, *4*(3), 329–352. https://doi.org/10.2307/622055

618 Horányi, A., Cardinali, C., Rennie, M. and Isaksen, L. (2015), The assimilation of horizontal
619 line-of-sight wind information into the ECMWF data assimilation and forecasting
620 system. Part I: The assessment of wind impact. *Quarterly Journal of the Royal*
621 *Meteorological Society*, 141: 1223-1232. https://doi.org/10.1002/qj.2430

622 Inoue, J., Yamazaki, A., Ono, J., Dethloff, K., Maturilli, M., Neuber, R., ... & Yamaguchi, H.
623 (2015). Additional Arctic observations improve weather and sea-ice forecasts for the
624 Northern Sea Route. *Scientific Reports*, *5*(1), 16868.

625 James, E. P., Benjamin, S. G., & Jamison, B. D. (2020). Commercial-Aircraft-Based
626 Observations for NWP: Global Coverage, Data Impacts, and COVID-19. *Journal of*
627 *Applied Meteorology and Climatology*, *59*(11), 1809-1825.
628 https://doi.org/10.1175/JAMC-D-20-0010.1

629 Jiang, Q. (2003). Moist dynamics and orographic precipitation. *Tellus A*: Dynamic Meteorology
630 and Oceanography, 55:4, 301-316, DOI: 10.3402/tellusa.v55i4.14577

631 Joe, P., Melo, S., Burrows, W. R., Casati, B., Crawford, R. W., Deghan, A., Gascon, G., Mariani,
632 Z., Milbrandt, J., & Strawbridge, K. (2020). The Canadian Arctic Weather Science
633 Project: Introduction to the Iqaluit Site. *Bulletin of the American Meteorological*
634 *Society*, *101*(2), E109-E128. https://doi.org/10.1175/BAMS-D-18-0291.1

635 Jung, T., Kasper, M. A., Semmler, T., & Serrar, S. (2014). Arctic influence on subseasonal
636 midlatitude prediction. *Geophysical Research Letters*, *41*(10), 3676-3680.

637 Jung, T., Gordon, N. D., Bauer, P., Bromwich, D. H., Chevallier, M., Day, J. J., Dawson, J.,
638 Doblas-Reyes, F., Fairall, C., Goessling, H. F., Holland, M., Inoue, J., Iversen, T., Klebe,
639 S., Lemke, P., Losch, M., Makshtas, A., Mills, B., Nurmi, P., Perovich, D., Reid, P.,

Renfrew, I. A., Smith, G., Svensson, G., Tolstykh, M., & Yang, Q. (2016). Advancing Polar Prediction Capabilities on Daily to Seasonal Time Scales. *Bulletin of the American Meteorological Society*, *97*(9), 1631-1647. https://doi.org/10.1175/BAMS-D-14-00246.1

Kim, G., Kim, J. & Cha, DH. (2022) Added value of high-resolution regional climate model in simulating precipitation based on the changes in kinetic energy. *Geosci. Lett.* **9**, 38. https://doi.org/10.1186/s40562-022-00247-6

Kiriakidis, P., Gkikas, A., Papangelis, G., Christoudias, T., Kushta, J., Proestakis, E., Kampouri, A., Marinou, E., Drakaki, E., Benedetti, A., Rennie, M., Retscher, C., Straume, A. G., Dandocsi, A., Sciare, J., and Amiridis, V. (2023). The impact of using assimilated Aeolus wind data on regional WRF-Chem dust simulations. *Atmos. Chem. Phys.*, 23, 4391–4417. https://doi.org/10.5194/acp-23-4391-2023

Laroche, S. & Poan, E.D. (2021). Impact of the Arctic observing systems on the ECCC global weather forecasts. *Quarterly Journal of the Royal Meteorological Society*, 148(742), 252–271. https://doi.org/10.1002/qj.4203

Laroche, S. & St-James, J. (2022) Impact of the Aeolus Level-2B horizontal line-of-sight winds in the Environment and Climate Change Canada global forecast system. *Quarterly Journal of the Royal Meteorological Society*, 148(745), 2047–2062. https://doi.org/10.1002/qj.4300

Lawrence, H, Bormann, N, Sandu, I, Day, J, Farnan, J, Bauer, P. (2019). Use and impact of Arctic observations in the ECMWF Numerical Weather Prediction system. *Quarterly Journal of the Royal Meteorological Society*,145: 3432–3454. https://doi.org/10.1002/qj.3628

Lawrence, Z. D., Perlwitz, J., Butler, A. H., Manney, G. L., Newman, P. A., Lee, S. H., & Nash, E. R. (2020). The remarkably strong Arctic stratospheric polar vortex of winter 2020: Links to record-breaking Arctic Oscillation and ozone loss. *Journal of Geophysical Research: Atmospheres*, 125, e2020JD033271. https://doi.org/10.1029/2020JD033271

Le Marshall, J., Jung, J., Zapotocny, T., Redder, C., Dunn, M., Daniels, J., & Riishojgaard, L. P. (2008). Impact of MODIS atmospheric motion vectors on a global NWP system. *Australian Meteorological Magazine*, 57, 45–51.

Liu, B., Guo, J., Gong, W., Shi, L., Zhang, Y., & Ma, Y. (2020). Characteristics and performance of wind profiles as observed by the radar wind profiler network of China. *Atmospheric Measurement Techniques*, *13*(8), 4589-4600.

Martinez, C., Goddard, L., Kushnir, Y. *et al.* (2019). Seasonal climatology and dynamical mechanisms of rainfall in the Caribbean. *Clim Dyn* **53**, 825–846. https://doi.org/10.1007/s00382-019-04616-4

Martin, A., Weissmann, M., and Cress, A. (2023). Investigation of links between dynamical scenarios and particularly high impact of Aeolus on numerical weather prediction (NWP) forecasts. *Weather Climate Dynamics*, 4, 249–264. https://doi.org/10.5194/wcd-4-249-2023

Mattingly, K. S., Ramseyer, C. A., Rosen, J. J., Mote, T. L., and Muthyala, R. (2016), Increasing water vapor transport to the Greenland Ice Sheet revealed using self-organizing maps. *Geophys. Res. Lett.*, 43, 9250–9258. https://doi.org/10.1002/2016GL070424

McTaggart-Cowan, R., Vaillancourt, P. A., Zadra, A., Chamberland, S., Charron, M., Corvec, S., et al. (2019). Modernization of atmospheric physics parameterization in Canadian

NWP. *Journal of Advances in Modeling Earth Systems*, 11, 3593–3635. https://doi.org/10.1029/2019MS001781

Mile, M., Azad, R., & Marseille, G.-J. (2022). Assimilation of Aeolus Rayleigh-clear winds using a footprint operator in AROME-Arctic mesoscale model. *Geophysical Research Letters*, 49, e2021GL097615. https://doi.org/10.1029/2021GL097615

Misra, V., DiNapoli, S., & Powell, M. (2013). The Track Integrated Kinetic Energy of Atlantic Tropical Cyclones. *Monthly Weather Review*, *141*(7), 2383-2389. https://doi.org/10.1175/MWR-D-12-00349.1

Mizyak, V. G., Shlyaeva, A. V., & Tolstykh, M. A. (2016). Using satellite-derived Atmospheric Motion Vector (AMV) observations in the ensemble data assimilation system. Russian Meteorology and Hydrology, 41, 439-446. https://doi.org/10.3103/S1068373916060091

Naakka, T., Nygård, T., Tjernström, M., Vihma, T., Pirazzini, R., & Brooks, I. M. (2019). The impact of radiosounding observations on numerical weather prediction analyses in the Arctic. *Geophysical Research Letters*, 46, 8527–8535. https://doi.org/10.1029/2019GL083332

Olaguera, L.M.P., Caballar, M.E., De Mata, J.C. *et al.* (2021). Synoptic conditions and potential causes of the extreme heavy rainfall event of January 2009 over Mindanao Island, Philippines. *Nat Hazards* **109**, 2601–2620. https://doi.org/10.1007/s11069-021-04934-z

Overland, J., Francis, J. A., Hall, R., Hanna, E., Kim, S., & Vihma, T. (2015). The Melting Arctic and Midlatitude Weather Patterns: Are They Connected?. *Journal of Climate*, *28*(20), 7917-7932. https://doi.org/10.1175/JCLI-D-14-00822.1

Palmén, E. (1958), Vertical Circulation and Release of Kinetic Energy during the Development of Hurricane Hazel into an Extratropical Storm. *Tellus*, 10: 1-23. https://doi.org/10.1111/j.2153-3490.1958.tb01982.x

Pourret, V., Šavli, M., Mahfouf, J.-F., Raspaud, D., Doerenbecher, A., Bénichou, H., et al. (2022) Operational assimilation of Aeolus winds in the Météo-France global NWP model ARPEGE. *Quarterly Journal of the Royal Meteorological Society*, 148(747), 2652–2671. https://doi.org/10.1002/qj.4329

Radić, V., Cannon, A. J., Menounos, B., and Gi, N. (2015), Future changes in autumn atmospheric river events in British Columbia, Canada, as projected by CMIP5 global climate models. *J. Geophys. Res. Atmos.*, 120, 9279–9302. https://doi.org/10.1002/2015JD023279

Randriamampianina, R., Bormann, N., Køltzow, M. A., Lawrence, H., Sandu, I., & Wang, Z. Q. (2021). Relative impact of observations on a regional Arctic numerical weather prediction system. *Quarterly Journal of the Royal Meteorological Society*, *147*(737), 2212-2232.

Randriamampianina, R., Schyberg, H., & Mile, M. (2019). Observing System Experiments with an Arctic Mesoscale Numerical Weather Prediction Model. *Remote Sensing*, *11*(8), 981. https://doi.org/10.3390/rs11080981

Rani, S. I., Sharma, P., George, J. P., & Das Gupta, M. (2021). Assimilation of individual components of radiosonde winds: An investigation to assess the impact of single-component winds from space-borne measurements on NWP. *Journal of Earth System Science*, *130*(2), 89.

Rennie, M.P., Isaksen, L., Weiler, F., de Kloe, J., Kanitz, T. & Reitebuch, O. (2021). The impact of Aeolus wind retrievals on ECMWF global weather forecasts. *Quarterly Journal of the Royal Meteorological Society*, 147(740), 3555–3586. https://doi.org/10.1002/qj.4142

Reynolds, C. A., Crawford, W., Huang, A., Barton, N., Janiga, M. A., McLay, J., Flatau, M., Frolov, S., & Rowley, C. (2022). Analysis of Integrated Vapor Transport Biases. *Monthly Weather Review, 150*(5), 1097-1113. https://doi.org/10.1175/MWR-D-21-0198.1

Smith, G. C., Bélanger, J., Roy, F., Pellerin, P., Ritchie, H., Onu, K., Roch, M., Zadra, A., Colan, D. S., Winter, B., Fontecilla, J., & Deacu, D. (2018). Impact of Coupling with an Ice–Ocean Model on Global Medium-Range NWP Forecast Skill. *Monthly Weather Review*, *146*(4), 1157-1180. https://doi.org/10.1175/MWR-D-17-0157.1

Tan, X., Gan, T.Y., & Chen, Y.D. (2019). Synoptic moisture pathways associated with mean and extreme precipitation over Canada for summer and fall. *Clim Dyn* **52**, 2959–2979. https://doi.org/10.1007/s00382-018-4300-6

Velden, C. S., Hayden, C. M., Nieman, S. J., Menzel, W. P., Wanzong, S., & Goerss, J. S. (1997). Upper-tropospheric winds derived from geostationary satellite water vapor observations. *Bulletin of the American Meteorological Society*, 78, 173–195. https://doi.org/10.1175/1520-0477(1997)078,0173:UTWDFG.2.0.CO;2

Velden, C., Lewis, W. E., Bresky, W., Stettner, D., Daniels, J., & Wanzong, S. (2017). Assimilation of High-Resolution Satellite-Derived Atmospheric Motion Vectors: Impact on HWRF Forecasts of Tropical Cyclone Track and Intensity. *Monthly Weather Review*, 145, 1107-1125. https://doi.org/10.1175/MWR-D-16-0229.1

748 Young, I. R., Sanina, E., & Babanin, A. V. (2017). Calibration and Cross Validation of a Global
749 Wind and Wave Database of Altimeter, Radiometer, and Scatterometer Measurements.
750 *Journal of Atmospheric and Oceanic Technology*, 34, 1285-1306.

751 Zuo, H. and Hasager, C. B. (2023). The impact of Aeolus winds on near-surface wind forecasts
752 over tropical ocean and high-latitude regions. *Atmospheric Measurement Technique*, 16,
753 3901-3913. https://doi.org/10.5194/amt-16-3901-2023

Aeolus winds improve Arctic weather prediction

C.-C. Chou[1], P. J. Kushner[1], and Z. Mariani[2]

[1]Department of Physics, University of Toronto, Toronto, M5S 1A7, Canada

[2]Meteorological Research Division, Environment and Climate Change Canada, Toronto, Canada

Corresponding author: Chih-Chun Chou (gina.chou@mail.utoronto.ca)

Key Points:

- Operational wind products are a key component of skillful numerical weather prediction in the Arctic.
- Augmenting operational winds with Aeolus winds could enhance the forecasts of winds and temperature fields by 14-18%.
- Aeolus wind improvements are most pronounced on strong wind days.

Abstract

It has been proven that assimilating winds from the Aeolus global Doppler wind lidar would enhance the predictive skill of weather forecast models. In this study, we use a series of Observing System Experiments to examine how operational winds and Aeolus winds impact Environment and Climate Change Canada's global forecast system over the data-sparse Arctic region. Aeolus winds improve the tropospheric wind and temperature forecasts by about 0.7 to 0.9% of error reduction (a 15-20% effect compared to the impact of operational wind products), while having little impact on the specific humidity field. In particular, Aeolus winds have an impact on forecasts of strong wind days on the wind and temperature fields that is double the impact of the forecasts of less intense wind days and provides a disproportionate improvement to forecasts on these days compared to other operational wind measurements. These findings suggest significant potential for global doppler wind lidar observations to enhance severe-weather prediction in polar regions.

Plain Language Summary

Wind observations are necessary to produce accurate weather forecasts. Aeolus is a new satellite that provides the first global wind profile measurements and it has a proven positive impact on forecasts. In this study, we investigate the impact of a large set of wind observations, including Aeolus winds, on Arctic weather forecasts using Canada's main forecast. We can calculate how these wind observations improve the forecast throughout the atmosphere, and find that Aeolus winds further improve the forecast in the lower atmosphere. Furthermore, our findings highlight the heightened significance of wind observations in ensuring precise forecasts of strong wind days. The difference is about double the improvement on the forecast of less intense wind days. This suggests that future doppler wind lidar programs following from Aeolus could significantly

benefit forecast skill in data-sparse regions like the Arctic and Antarctic, which are of growing societal, political, and economic interest.

1 Introduction

Arctic weather forecasts produced by operational numerical weather prediction (NWP) models present unique challenges (Bauer et al., 2016; Jung et al., 2016; Gascard et al., 2017). The Arctic presents unique logistical and environmental challenges that hinder real-time data collection and the maintenance of observation equipment (Randriamampianina et al., 2019; Lawrence et al., 2019; James et al., 2020; Joe et al., 2020; Chou et al., 2020). Furthermore, the Arctic's unique geography and rapidly changing climate contribute to unpredictable and extreme weather events (Cohen et al. 2014; Francis et al., 2017; Lawrence et al., 2019; Eikeland et al., 2022). Nevertheless, improving Arctic forecasts remains imperative for the safety of residents and travellers in the region. Furthermore with melting sea ice opening up new opportunities, the Arctic is gaining increasing importance for shipping and industry (Gascard et al., 2017; Eicken, 2013; Inoue et al., 2015). Finally, given implications of Arctic change for have sea level rise and altered weather patterns, accurate forecasts promises to improve our understanding of and ability to adapt to climate change (Cohen et al. 2014; Jung et al., 2014; Overland et al. 2015; Francis et al., 2017; Laroche and Poan, 2021).

An essential element in producing reliable forecasts is the initialization of NWP systems with precise and timely observational data (Inoue et al., 2015; Randriamampianina et al., 2021). These observations allow estimation of the present atmospheric state, enabling the NWP system to establish the initial conditions necessary for accurate forecasts. Wind is a fundamental component of atmospheric dynamics, influencing the movement of air masses, the formation and evolution of weather systems, and the transport and advection of heat, moisture, and other

atmospheric constituents (Baker et al., 1995; Graham et al., 2000; Naakka et al., 2019). Thus, wind observations play a pivotal role in NWP initialization, even after accounting for the balance that constrains winds given pressure and temperature measurements (Horányi et al., 2014; Naakka et al., 2019; James et al., 2020).

Observations of altitude-resolved winds are available through aircraft reports (AMDAR; Dai et al., 2014; James et al., 2020), radiosondes (Durre et al., 2018; Carminati et al., 2019; Rani et al., 2021), and wind profiling technologies (e.g., Doppler radar and lidar; Augustine and Zipser, 1987; Rogers et al., 1993; Liu et al., 2020). However, these observations are often sporadic and notably scarce, particularly over vast bodies of water like oceans and the polar regions. Passive space-based observations offer an alternative, with Atmospheric Motion Vectors (AMVs) estimating wind speed and direction based on cloud and water vapor movements (Velden et al., 2017; Mizyak et al., 2016). Additionally, space-based scatterometers provide surface winds over the ocean. Despite the advantages of AMVs in offering wind information across multiple tropospheric layers through multispectral water vapor remote sensing (Velden et al., 1997; Bormann and Thépaut, 2004; Le Marshall et al., 2008), they lack precision in altitude assignment and are limited to a few levels, hindering their representation of small-scale vertical wind profile structures. Conversely, spaceborne scatterometers focus only on near-surface ocean winds, with their accuracy highly dependent upon surface weather conditions (Chiara et al., 2017; Young et al., 2017).

The Aeolus mission, featuring the first spaceborne Doppler Wind Lidar (DWL), provides the first-ever global horizontal line-of-sight (HLOS) wind profile measurements. Studies have demonstrated that assimilating Aeolus HLOS winds into NWP systems significantly enhances forecast accuracy. Examples of operational forecast systems include those of ECMWF (Rennie

et al., 2021), NCMRWF (George et al., 2021), DWD (Martin et al., 2023), NOAA (Garrett et al., 2022), Météo-France (Pourret et al., 2022), and Environment and Climate Change Canada (ECCC; Laroche and St-James, 2022). Most of the improvements were found in the tropical troposphere to lower stratosphere. Notably, Aeolus winds have also demonstrated a beneficial impact on forecasts in data-sparse regions such as the Southern Hemisphere extra-tropics and the Arctic (Mile et al., 2022; Chou and Kushner, 2023; Zuo and Hasager, 2023).

Despite the good coverage that polar-orbiting satellites provide over the Arctic, more than 90% of the assimilated observations over the Arctic are microwave and infrarared radiances (Lawrence et al., 2019; Randriamampianina et al., 2021). As previously discussed, wind observations from conventional surface and aircraft measurements are extremely sparse in this region. Hence, it is important to assess the impact of existing wind observations and any additional wind observations over the Arctic to compare and determine their impact on NWP model performance over the Arctic.

In this study, we extend the work of Chou and Kushner (2023) and evaluate the impact of operational winds and Aeolus winds on the global forecast system of ECCC with a focus on the Arctic. Chou and Kushner (2023) used a series of Observing System Experiments (OSE), in which all operational winds or Aeolus winds are withheld in the assimilation and the forecasts are verified against the fifth-generation European Centre for Medium-Range Weather Forecasts (ECMWF) atmospheric reanalysis (ERA5, Hersbach et al., 2023). The integration of operational winds significantly enhanced tropospheric wind forecasts, particularly in tropical regions, resulting in an impressive 8% reduction in forecast error. Further augmenting these assimilations with Aeolus winds contributed an additional 0.7-0.9% improvement or about 10% of the impact of operational winds. Notably, Aeolus winds also proved beneficial in regions with limited data,

such as the Arctic and the extra-tropical Southern Hemisphere, demonstrating a reduction in forecast errors ranging from 0.5% to 0.9%. While operational winds contribute significantly to forecast improvement, unexpected occurrences such as the COVID-19 pandemic can disturb aircraft measurements, resulting in less precise forecasts during such periods (James et al., 2020). This circumstance, and the need to quantify Doppler wind lidar profiles' impact in isolation from other wind-observation systems, prompts the addition of this study's OSE labeled "CNTRL–wind+Aeolus" (refer to Section 2 for the experimental setup). This new OSE aims to specifically assess the isolated impact of Aeolus winds in the Arctic without the influence of other wind products.

Our investigation encompasses an assessment of the overall improvements in Arctic forecasts resulting from the assimilation of different sets of wind observations, as well as an exploration of the influence of wind observations on the forecasts related to enhanced kinetic energy and intense Integrated Vapor Transport (IVT). Henceforth, "disturbed" atmospheric state is used to describe days with strong winds or intense vapor transport. These two metrics were selected because of their large societal and economic impacts. Enhanced kinetic energy is commonly used as a severe-weather indicator, e.g. for severe storms, tornadoes, hurricanes, and typhoons (Palmén, 1958; DeMego and Bosart, 1982; Misra et al., 2013; Bass et al., 2017) and as an indirect indicator of extreme rainfall and flooding events (Brodie and Rosewell, 2007; Chang et al., 2017; Kim et al., 2022). Energetic systems can also transport substantial moisture from moisture sources, which can lead to weather-related water damage (Hills, 1978; Jiang, 2003; Chen et al., 2012; Martinez et al., 2019; Olaguera et al., 2021). Recent research suggests that ongoing climate changes are likely modifying IVT patterns, influencing the frequency and

intensity of future extreme weather events (Radic et al., 2015; Mattingly et al., 2016; Gershunov et al., 2017; Tan et al., 2019).

This paper is organized as follows: Section 2 outlines the experimental setup, including details on the ECCC global forecast system and OSE. In Section 3, we present impact scores by comparing forecasts to ERA5 and define strong wind and strong vapor transport events. Section 4 unveils our results on the impact of wind observations on forecasts over the Arctic and on atmospheric events in the region. Finally, Section 5 offers a discussion of the main conclusions derived from this study.

2 Experimental Setup

OSEs are used to evaluate and assess the impact of observational data on NWP models by adding or removing a set of observations that are assimilated into the NWP model (Bouttier and Kelly, 2001; Laroche and Poan, 2021; Laroche and St-James, 2022). In this study, we use an extension of the series of OSEs used in Chou and Kushner (2023) to examine the impact of the operational wind observations and of Aeolus HLOS winds on the Arctic forecasts of the Canadian Global Deterministic Prediction System (GDPS). The OSEs cover two seasons: from July 1 to September 30 2019 (summer 2019) and from December 1 2019 to March 31 2020 (winter 2020). The atmospheric component of the forecast system is the latest version of the operational Global Environmental Multiscale (GEM) model implemented at ECCC in 2019 (McTaggart-Cowan et al., 2019) and the ocean component of the forecast system is the NEMO ocean model (Smith et al., 2018). The model uses approximately 15 km horizontal grid spacing and 84 vertical levels. The data assimilation scheme is the operational four-dimensional ensemble-variational (4D-EnVar) (Buehner et al., 2015) system, with a 6-h assimilation window which includes over 13 million observations assimilated daily. Two forecasts were generated

daily (at 00 and 12 UTC). To minimize the computational cost, a coarser horizontal grid resolution of 39 km is employed and some aspects of the GEM physics are simplified. Implications of the use of this coarse resolution will be discussed in Section 5. Further details and justification on this simplified GDPS version are provided in Laroche and St-James (2022) and Chou and Kushner (2023). To examine the impact of wind observations, four experiments are carried out:

1. CNTRL, an experiment with all operational observations.
2. CNTRL–winds (i.e., "control-minus-winds"), an experiment with all operational observations except the operational wind observations. Operational winds include wind measurements from AMDAR, AMVs, radiosondes, surface stations, surface buoys, wind profilers, and scatterometry. This assesses the impact of all operational wind products on NWP skill.
3. CNTRL–wind+Aeolus (i.e., "control-minus-winds-plus-Aeolus"), an experiment with all operational observations and Aeolus HLOS winds (both Rayleigh-clear and Mie-cloudy winds) but without the operational wind observations. The winds used are from the second reprocessed product, the Level-2B11 product. This tests the impact of Aeolus winds in isolation from the other wind products and provides an assessment of NWP performance if traditional wind observations were halted (such as the reduction in AMDAR flights during Covid 19) but Aeolus was assimilated.
4. CNTRL+Aeolus (i.e., "control plus Aeolus"), an experiment that adds the Aeolus HLOS winds (both Rayleigh-clear and Mie-cloudy winds) to the CNTRL experiment. This tests the impact of Aeolus winds on top of the other wind products and provides an assessment of NWP performance if Aeolus winds were operationally assimilated.

Chou and Kushner (2023) used OSEs 1, 2, and 4. The current study is the first to use OSE 3 to test the effect of Aeolus wind impacts separately from other wind products.

To evaluate the impact of the wind observations, we compare the forecast root-mean-square error (RMSE) between the experiments. The mathematical expression of the forecast impact scores will be discussed in Section 3. Henceforth, the expression "impact of operational winds" (IOW) refers to the normalized change in the forecast scores from the CNTRL compared to the CNTRL–winds (i.e., error of CNTRL–winds minus error of CNTRL, which is therefore positive for improvement), the expression "impact of Aeolus winds" (IAW) refers to the change in the forecast scores from the CNTRL–winds+Aeolus compared to the CNTRL–winds (i.e., error of CNTRL–winds minus error of CNTRL–winds+Aeolus, which is therefore, again, positive for improvement), and the expression "impact of Aeolus on top of operational winds" (IAOW) refers to the change from the CNTRL+Aeolus compared to the CNTRL (i.e., error of CNTRL minus error of CNTRL+Aeolus, so, again, positive for improvement).

3 Method

We verify the forecasts from OSEs described in Section 2, against ERA5 from ECMWF (Hersbach et al., 2023). ERA5 is based on a four-dimensional variational (4DVar) data assimilation scheme using Cycle 41r2 of the Integrated Forecast System (IFS). We use the hourly winds, temperature, and specific humidity at 00 and 12 UTC. The data are gridded on a regular latitude-longitude grid of 0.25°, but linearly interpolated onto grid of 0.5° to match the coarser resolution of the OSEs, and only the OSEs' 16 pressure levels are selected (10, 20, 30, 50, 70, 100, 150, 200, 250, 300, 400, 500, 700, 850, 925, and 1000 hPa).

The impact of wind observations is defined as the normalized change (percentage change) in the forecast RMSE between the experiments over the Arctic. The steps to calculate the forecast RMSE are as follows:

1. Calculate the cosine-weighted mean-square-error (MSE) between the forecasts from OSEs and the verification field from ERA5, over the Arctic (70° to 90°N), for each forecast hour (two forecasts daily for a total of seven months). The MSE for a scalar field x (i.e., temperature, specific humidity, and IVT) is

$$MSE = \frac{\sum_i w_i \left(x_f - x_v\right)_i^2}{\sum_i w_i} \quad (1)$$

   and the MSE for a vector field $\vec{v}$ (i.e., vector wind and wind shear) is

$$MSE_{vector} = \frac{\sum_i w_i ||\vec{v}_f - \vec{v}_v||_i^2}{\sum_i w_i}. \quad (2)$$

   The index i indicates a grid point along a latitude band, the subscript f indicates the forecast, and the subscript v indicates the verification field. The weight $w_i = \cos\theta_i$, where θ_i is the latitude at location i.
2. The weighted MSEs are averaged over the seven months covering the available Aeolus observation products.
3. The square-root of the averaged weighted MSEs is the RMSE at each pressure level.
4. The normalized change in scores represents the percentage change of the RMSE between a pair of OSEs from Step 3.

5. The tropospheric impact score is the averaged scores from Step 4 from the four pressure levels: 850 hPa, 500 hPa, 250 hPa, and 100 hPa.

As introduced in Section 2, the impact of operational winds (IOW) is the percentage difference of forecast RMSE between CNTRL and CNTRL–winds; the impact of Aeolus winds (IAW) is the percentage difference of CNTRL–winds+Aeolus and CNTRL–winds; the impact of Aeolus on top of operational winds (IAOW) is the percentage difference of CNTRL+Aeolus and CNTRL.

Chou and Kushner (2023) show that adding Aeolus winds into data assimilation, which are the first global wind profile measurements, can improve the forecasts of the vertical structure of the wind field. We carry out this analysis in this study and will investigate the impact of wind observations on Arctic weather events on the tropospheric wind vector, temperature, wind shear (thermal-wind) vector (defined as the vector wind difference between 250 hPa and 850 hPa), specific humidity, and IVT. Analysis of specific humidity was included to help interpret the results of the IVT analysis.

For the second part of the paper (Section 4.2), we will discuss the impact of wind observations over the Arctic when the atmosphere is disturbed (i.e., strong kinetic energy or intense IVT). In preliminary work, we have investigated the impact of wind observations on localized events, such as strong wind events at radiosonde stations over the Arctic and forecasts along Aeolus swaths. This analysis is not shown in this study because, due to the short period of the Aeolus mission and the coarse resolution of the OSE forecasts, there were not many individual local events to average over, and we found that the OSEs had limited ability to resolve smaller-scale atmospheric features associated with severe Arctic weather such as polar lows. Instead, to investigate the impact of wind observations on predictability of extreme Arctic

weather events, we focus on days in which the atmosphere is strongly disturbed over the entire Arctic. In particular, we examine the impact of wind observations on the forecasts of "strong" 500-hPa Kinetic Energy (KE500) days vs. "normal" KE500 days, and of strong IVT days vs. normal IVT days over the Arctic. The KE500 ($m^2 s^{-2}$) is

$$KE500 = \frac{1}{2}(u^2 + v^2) \tag{3}$$

where u and v are the 500-hPa zonal and meridional wind components, respectively. The IVT ($kgm^{-1}s^{-1}$) is

$$IVT = \sqrt{\left(\frac{1}{g}\int_{1000}^{300} qudp\right)^2 + \left(\frac{1}{g}\int_{1000}^{300} qvdp\right)^2} \tag{4}$$

where g is the gravitational acceleration, q is the specific humidity, u and v are the zonal and meridional winds, and the product of the specific humidity and the winds is integrated over 1000, 925, 850, 700, 500, 400, and 300 hPa (Cordeira and Ralph, 2020; Reynolds et al., 2022).

We define the strong KE500 days and strong IVT days in a similar way. First, we define the threshold at each grid point as the 90th percentile of the local KE500 or the local IVT for the summer season and the winter season separately. We record the number of grid points poleward of 70°N that exceed this threshold and take the top 25% of this number for both seasons combined to get "strong weather-event days" with more disturbed atmospheric conditions. Trial and error suggests that this provides sufficient sampling to assess the impact of wind observations on the forecasts (Section 4.2).

4 Results

4.1 Impact of operational winds and Aeolus winds over the Arctic

Figure 1 shows the impact of operational winds (IOW), Aeolus winds (IAW), and Aeolus winds on top of operational winds (IAOW) on the tropospheric forecast RMSE over the Arctic. Note that the y-axis extends from -12 to 12% for the IOW (panel a) and from -4 to 4% for the IAW and IAOW (Figure 1b,c). As expected, operational wind observations notably enhance the forecasts of wind fields (vector wind and wind shear) and the temperature field, which provides a context for assessing the impacts of Aeolus (Chou and Kushner, 2023). Averaged scores for these three fields over five days demonstrate an improvement of approximately 5%. Replacing operational winds by Aeolus winds, IAW (Figure 1b), consistently delivers a positive impact of about 2%, constituting roughly 40% of the improvement achieved with all operational winds. It is noteworthy that Aeolus, despite being a single-satellite measurement system, contributes meaningfully to forecast enhancement.

Considering all operational winds, as reflected in the IAOW in Figure 1c, Aeolus winds further enhance the wind and temperature fields throughout the five-day forecast lead time by 0.7% and 0.9%, respectively, representing 14% to 18% of the overall improvement obtained with all operational winds. While this positive IAOW is relatively modest compared to improvements found by Aeolus for other models (e.g., Garrett et al., 2022; Rennie et al., 2021), it aligns with previous findings in OSEs conducted with the ECCC GDPS (Laroche and St-James, 2022; Chou and Kushner, 2023). The reasons for this modest impact are elaborated on in Chou and Kushner (2023). Despite the relatively small contribution, the impact of Aeolus winds on top of operational winds is noteworthy, particularly considering that Aeolus observations for this period constitute less than 1% of all operational wind observations. Notably, operational winds,

inclusive of measurements from various ground-based instruments, radiosondes, and satellites, account for roughly 10% of all operational observations over the Arctic in the ECCC GDPS. The lack of significance when assimilating Aeolus winds on top of operational winds might arise from the simplification and relatively coarse resolution of the ECCC model version used in this work to reduce computational cost, systematic model issues beyond this simplification, or assimilation system deficiencies, as discussed in Chou and Kushner (2023). Importantly, the IAW remains significant, reaching at least 90% confidence level, particularly in the wind fields for the first three days of the lead time.

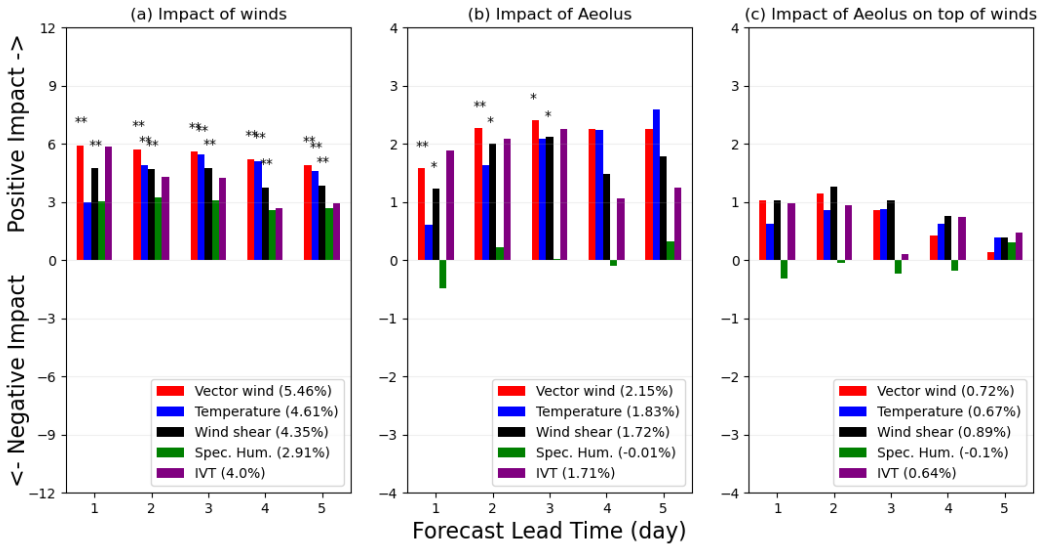

Figure 1: Normalized change in RMS forecast error between (a) CNTRL–winds and CNTRL (IOW), (b) CNTRL–winds and CNTRL–winds+Aeolus (IAW), and (c) CNTRL and CNTRL+Aeolus (IAOW), compared to ERA5 in the troposphere for vector wind (red), temperature (blue), wind shear (black), specific humidity (green), and integrated vapor transport (IVT) (purple) in the troposphere (850-100hPa layer) for 5-day forecasts over the Arctic. Positive impact means a reduction in the forecast error. The impacts that are significant at 95% confident level are marked with double asterisk (**) and impacts that are significant at 90% confident level are marked with single asterisk (*). The significance is tested using a t-test for the null hypothesis that the pair of experiments have identical cosine-

weighted RMSE from all four layers. The averaged impact over the five forecast lead time days is shown in the brackets.

Both operational winds and Aeolus winds show minimal to no impact on the specific humidity field, despite enhancements in other fields. The averaged IOW in Figure 1a over a five-day forecast lead time is approximately 3%, which is about half of the impact observed in the vector wind field. The IAW in Figure 1b and the IAOW in Figure 1c on the specific humidity field lack consistency throughout the forecast lead time. Consequently, the impact on the IVT, encompassing both wind and specific humidity information, falls between the impact on the wind fields and the specific humidity field. The averaged scores for the IVT are 4.0, 1.7, and 0.6% for the IOW, IAW, and IAOW, respectively.

Figure 2 provides a view of the spatial structure of the impact of wind observations on the vector wind field by breaking down the pressure-level and forecast lead time dependence (up to day 10). The tropospheric impacts observed in the first five days of the forecast lead time align with the findings depicted in Figure 1. Note that the color scale is compressed by factors of two when transitioning from the IOW in Figure 2a to the IAW in Figure 2b, and to the IAOW in Figure 2c. This demonstrates, consistently with Figure 1, that IAW contributes to about half of the improvement obtained by all operational winds. In the case of tropospheric IAOW, the enhancements from Aeolus winds on top of operational winds exceed 25% of the improvement obtained with all operational winds in short-range forecasts and are slightly less than 20% in short- to medium-range forecasts.

Conversely, Figure 2 reveals a degradation in forecast skills when assimilating Aeolus in the stratosphere. As previously discussed in Chou and Kushner (2023), this issue may arise from

the simplification of the ECCC model version used to reduce computational costs, systematic model issues beyond this simplification, or deficiencies in the assimilation system.

Overall, Figure 2 underscores the potential of Aeolus to enhance medium- to long-range forecasts, particularly in the upper atmosphere beyond day 4. The IAW accounts for more than 50% of the improvements from operational winds, and more than 25% for the IAOW. This stratospheric improvement in long-range forecasts over the Arctic is primarily attributed to the signal during the winter season, characterized by an anomalously strong Arctic stratospheric polar vortex in 2019-2020 (Chou and Kushner, 2023; Lawrence et al., 2020).

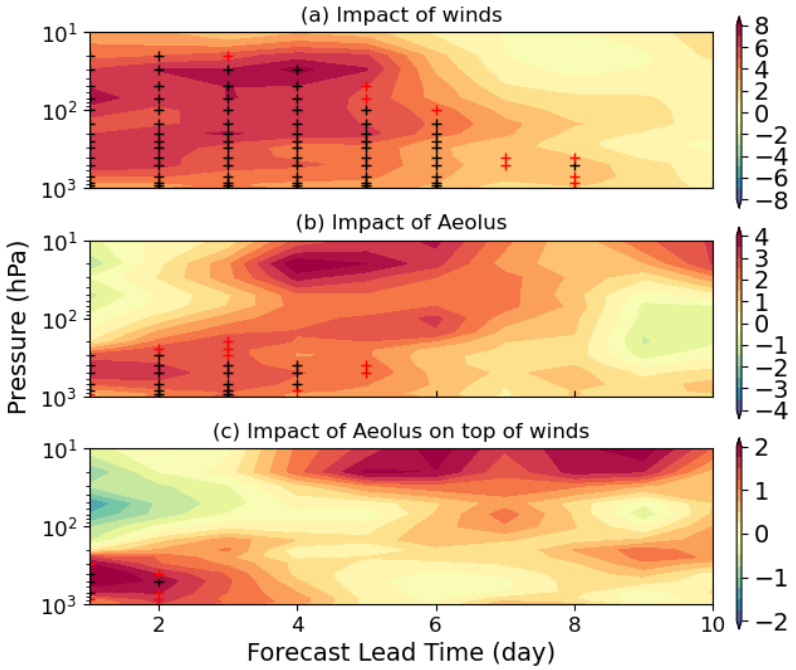

Figure 2: Normalized change in RMS forecast error as a function of pressure level between (a) CNTRL–winds and CNTRL, (b) CNTRL–winds and CNTRL–winds+Aeolus, and (c) CNTRL and CNTRL+Aeolus, for wind vector for 10-day forecasts over the Arctic. Positive impact means a reduction in the forecast error. The impacts that are significant at 95% confident level are marked with black plus sign and impacts that are significant at 90% confident

level are marked with red plus sign. The scores with respect to ERA5 data are interpolated onto the 16 pressure levels of the OSEs.

Despite previous challenges in attributing improvements in the Arctic forecast to localized regions, some regional insight can be gained by including all forecasts and dividing the Arctic into quadrants. We repeat the pan-Arctic analysis for four Arctic quadrants and investigate the IOW, IAW, and IAOW on the wind and temperature fields over each quadrant (SFigures 1 to 3 respectively). This shows that over the Arctic, Russian-Pacific-Northern Canada sector forecasts (90°E –180°E and 180°E–270°E) are most improved and sensitive to the wind observations; the IOW on the vector wind field are 5.7% and 6.7%, compared to 4.6% and 5.0% over the other two quadrants and similar results are found when Aeolus winds are assimilated. The IAW and IAOW on the vector wind field are around 2.7 and 0.8% respectively over the quadrants between 90° and 270°E, which are about 40 and 13% of the IOW, but the impacts are only around 1.6 and 0.6% over the other two quadrants, which are 33 and 12% compared to IOW. The reason why this region's forecasts are more sensitive to wind observations remains unclear, but it is consistent when different sets of wind observations are assimilated into the forecast model. There are many aspects that can lead to this difference; for example, the proportion of land, ocean, and snow/ice, number of observations over the region, and the physics used for the region in the model. However, such investigations are beyond the scope of this paper.

4.2 Impact of wind observations on strong wind and vapor transport events over the Arctic

We are interested in whether wind observations would improve the forecasts of severe weather events and how much in advance the forecasts would show an improvement. More

specifically, this subsection presents the impact of wind observations on strong wind events and water vapor transport events over the Arctic. The proportions of the Arctic that exceed the KE500 and IVT thresholds (90^{th} percentile of the field of the season) are recorded at each forecast hour and the time-series of this spatial coverage ratio are shown in Figures 3 and 4, respectively. The days that are defined as more energized or in a more disturbed atmospheric state are the top 25% (red dots) of this spatial coverage ratio during the entire period of analysis. For these events at and above the 75^{th} percentile, the forecasts that are defined as strong KE500 occur when at least 13% of the Arctic points exceed the thresholds of the field, and the forecasts that are defined as strong IVT occur when at least 12% of the Arctic exceed the threshold of the field. Strong KE500 forecasts do not necessarily overlap with the forecasts that have strong IVT. For example, before mid-July 2019, there are around eight forecasts that experienced strong IVT, but none of the forecasts during this period are defined as strong KE500 forecasts. Also, at the end of December 2019 and in early January 2020, most of the forecasts show an energetic, strong KE500, atmosphere, but the IVT over the Arctic during this period is relatively weak. By grouping the forecasts using the top 25%, we get sufficient forecasts (around 100 forecasts) to compare and to investigate the impact of wind observations on disturbed atmospheric states.

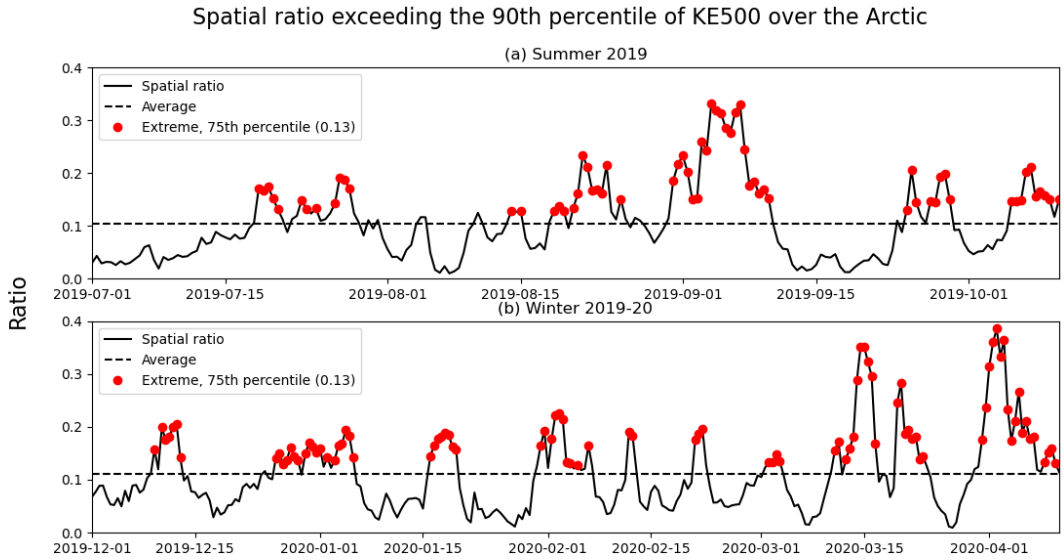

369

370 Figure 3: The time-series (solid black line) during (a) summer 2019 and (b) winter 2019-20 of the spatial coverage
371 ratio that exceeds the 90th percentile of the 500-hPa Kinetic Energy of the season over the Arctic. The time-averaged
372 of the spatial ratio of the season is shown as the dashed black line. The strong KE500 days (red dots) are defined as
373 when the spatial ratio exceeds the 75th percentile of the two seasons combined. The threshold of the spatial ratio (the
374 75th percentile) is indicated in the legend for the extreme days.

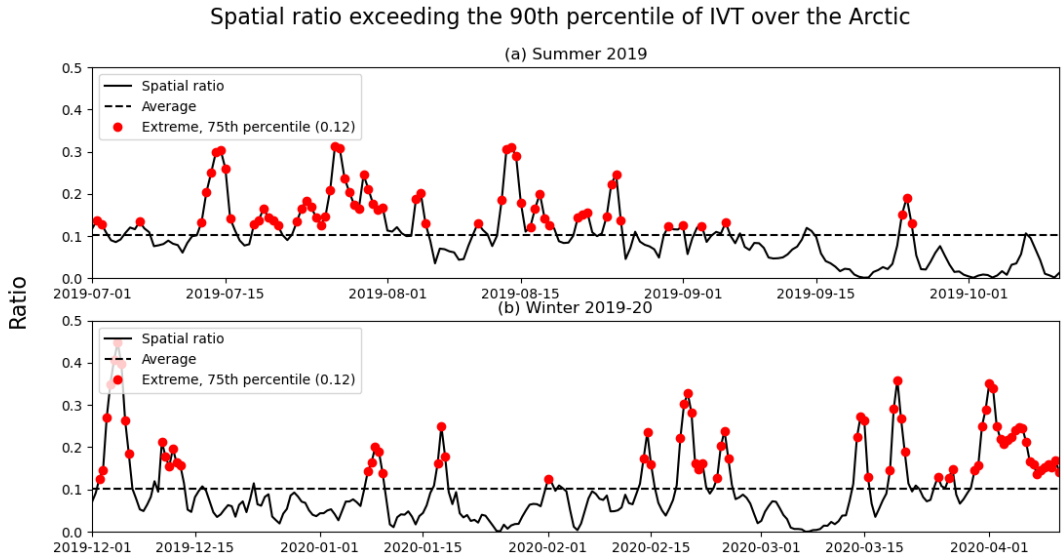

375

Figure 4: Similar to Figure 3, but for the spatial coverage ratio that exceeds the 90th percentile of the IVT over the Arctic.

We use the same approach, outlined in Section 3, to find the normalized change in the forecast RMSE between a pair of experiments, but we composite tropospheric forecast skill impacts conditioned on strong (Figure 5a,b,c) and normal (Figure 5d,e,f) Arctic KE500, and on strong (Figure 6a,b,c) and normal (Figure 6d,e,f) Arctic IVT. Note that the x-axis is showing the forecast "ahead" time, instead of the forecast lead time as shown in Figures 1 and 2. The forecast ahead time represents the number of days prior to the identified disturbed atmospheric day, as measured with KE500 or IVT. For instance, if there is a strong wind event on July 15th, then the scores show the impact of wind observations on forecasts of July 15th that were made prior to the event. If the score for forecasts of two-day ahead time is 2%, then it means that the forecast RMSE with two-day lead time that was made on July 13th is reduced by 2% when wind observations are assimilated.

The wind observations consistently provide more positive impact on forecasts of strong KE500 on wind and temperature fields. For example, the IOW on forecasts of normal KE500 is around 4.6% and it increases to around 5.8% when conditioned on forecasts of strong KE500. Consistent findings are noted with the assimilation of Aeolus winds. The impact scores show an increase from 1.8 to 2.4% when operational winds are replaced by Aeolus winds, when conditioned on normal (Figure 5e) and strong (Figure 5b) KE500 days. Specifically, the IAOW for forecasts of strong KE500 is nearly triple the impact scores observed when conditioned on normal KE500 days. The averaged scores over the five forecast lead times rise from 0.6 to 1.5%.

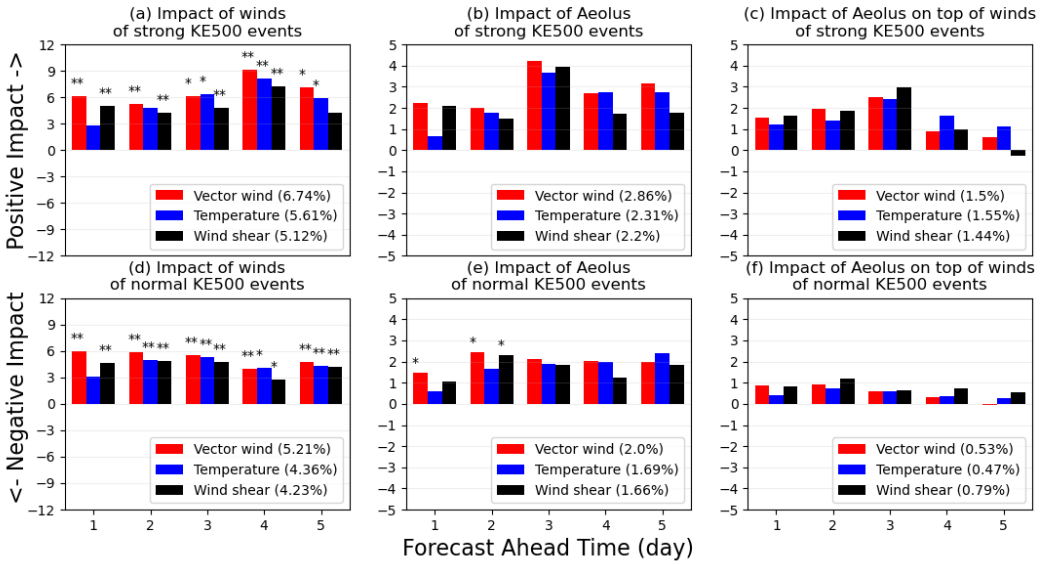

397

398 Figure 5: Normalized change in RMS forecast error for IOW (left column), IAW (middle column), and IAOW (right
399 column) for vector winds, temperature and wind shear, as a function of "Forecast Ahead Time" (see text), for strong
400 KE500 forecasts only (top row) and normal KE500 forecasts only (bottom row). Note that the scale of the y-axis
401 extends from -5 to 5% for panels b, c, e, and f. Significance testing as in Figure 1. Strong KE500 events are defined
402 in Figure 3; the remaining KE500 events are identified as "normal".

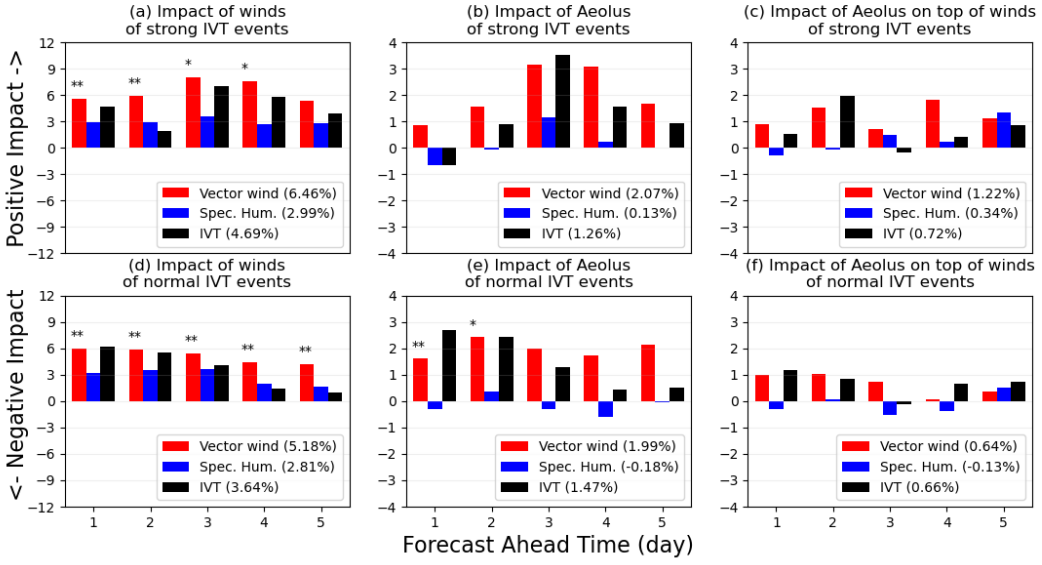

403

Figure 6: Similar to Figure 5, but for vector winds, specific humidity, and IVT, for strong and normal IVT events defined in Figure 4.

Greater impacts are also seen when conditioned on forecasts of strong IVT (Figure 6a,b,c) compared to forecasts of normal IVT (Figure 6d,e,f). The IOW on the wind field increases by approximately 1.3% when conditioned on strong IVT and by 1.0% for the IVT field. Conversely, the averaged IAW over five days shows little to no difference when conditioned on forecasts of strong IVT days (Figure 6b,e). The impact scores averaged over the five forecast lead times on the wind and IVT fields exhibit no more than a 0.2% difference. If Aeolus winds are assimilated on top of operational winds, the IAOW would approximately double the impact scores for the wind field when conditioned on forecasts of strong IVT (Figure 6c). Generally, Aeolus winds (Figure 6b,c,e,f) demonstrate little to no consistent impact on the specific humidity field.

The results from Figure 5 encourage us to investigate the profiles of impact of wind observations conditioned on strong (Figure 7a,c,e) and normal (Figure 7b,d,f) Arctic KE500 with a longer forecast ahead time. Profiles of impact conditioned on strong and normal Arctic IVT are shown in the supplementary information (SFigure 6). The operational winds reduce the forecast RMSE by more than 8% throughout the atmosphere with 3 to 5 days of lead time before strong KE500 days (Figure 7a), whereas they only reduce the forecast RMSE by about 4% for normal KE500 (Figure 7b). When operational winds are replaced by Aeolus winds, the IAW on forecasts of strong KE500 with a lead time of 3 to 5 days (Figure 7c) accounts for approximately 50% of the improvement obtained with all operational winds. Consistently with our findings above, the IAW is about 40% of the IOW and the IAW impact on strong KE500 days is greater than on normal KE500 days (Figures 7c-d), and IAOW is about 25% of the IOW, with extended lower

tropospheric impacts four or more days ahead being evident for the strong KE500 days, which is not as evident for the normal KE500 days (Figures 7e-f).

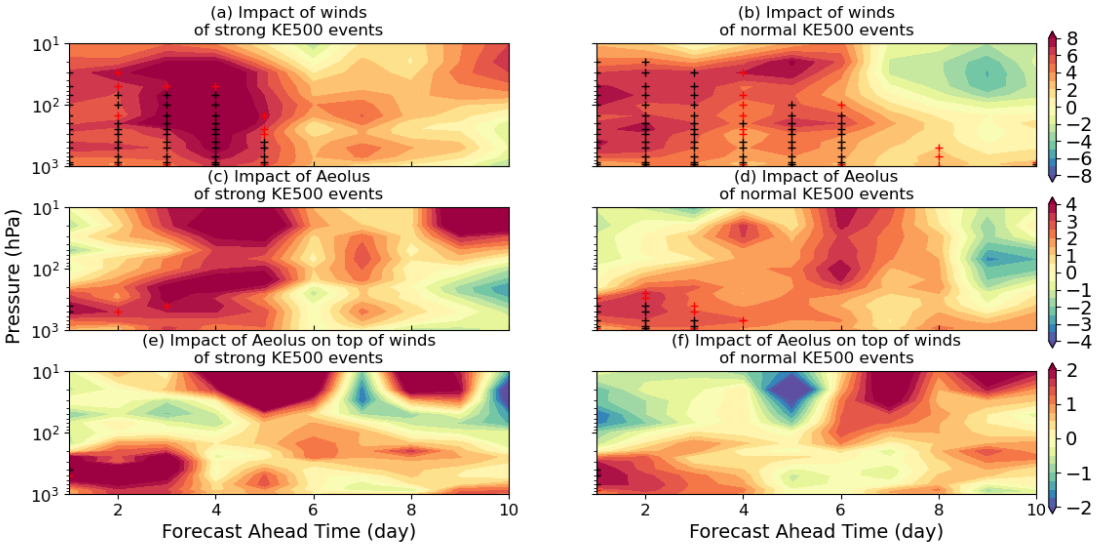

Figure 7: Normalized change in RMS forecast error as a function of pressure level for IOW (top row), IAW (middle row) and IAOW (bottom row), for wind vector errors up to 10 forecast days ahead. Positive impact means a reduction in the forecast error. The left column shows the impact of the added wind observations respectively of the strong KE500 days only defined in Figure 3 and column two shows the impact of the non-strong KE500 days only. Significance testing as in Figure 2.

5 Conclusions

The Arctic has fewer weather observation stations and limited data sources due to its low population density, limited accessibility, and harsh environment. However, the Arctic's distinctive geography, increasing economic activity, global geopolitical importance, and rapidly evolving climate changes necessitate advances in weather modeling and forecasting. Precise weather predictions in the Arctic are crucial for the safety of individuals and navigation in the area, and a deeper comprehension of Arctic weather has the potential to improve global climate models.

To better understand the role of wind observations in the weather forecasts over the Arctic, we have assessed the impact of operational winds (IOW), Aeolus winds (IAW), and Aeolus winds on top of operational winds (IAOW) on the ECCC global forecast system over the Arctic during July to September 2019 and December 2019 to March 2020. The analysis covers both the difference between disturbed atmospheric conditions (high versus normal KE500 and IVT days) and surveys different Arctic sectors for improvements. This extends Chou and Kushner (2023) who examined the general scale dependence and global distribution of IOW and IAOW. The IAOW has been enabled by the new experiment without the operational winds but with the Aeolus winds (CNTRL–winds+Aeolus), which allows us to study the impact of Aeolus winds as if it were, hypothetically, the only source of wind observations.

As anticipated, operational winds significantly enhance Arctic forecasts, reducing forecast RMSE by approximately 5%, particularly in the wind and temperature fields. This improvement is even greater for disturbed atmospheric conditions, as measured by high KE500 and IVT values. This highlights how wind observations become even more important during extreme atmospheric states where simple dynamical balances that couple mass and circulation break down. Despite Aeolus winds representing less than 1% of operational wind observations, substituting operational winds with Aeolus winds in the assimilation process results in an observed 2% reduction in errors, equivalent to approximately 40% of the improvement achieved by operational winds. This improvement extends to the additional forecast improvements seen on strong KE500 and IVT days. Thus, despite being derived from a single satellite, Aeolus winds can match nearly half of the forecast enhancement realized by operational winds, which incorporate wind measurements from multiple ground-based instruments, radiosondes, and satellites. This suggests that Doppler wind lidar systems have the potential to strongly

complement conventional wind observations. This was already seen when Aeolus data was shown, during the COVID-19 pandemic, to be capable of compensating for the disruption of AMDAR aircraft wind measurements and consequent forecast degradation (James et al., 2020). Altogether, assimilating Aeolus winds on top of operational winds (IAOW) yields an additional 0.8% reduction in errors, constituting around 16% of the overall improvement obtained with all operational winds.

While wind observations exhibit positive outcomes for mass-related fields like temperature, operational winds only contribute approximately half of the impact on the specific humidity field compared to the temperature field. Additionally, both the IAW and IAOW show little to no influence on the specific humidity field over the Arctic. This suggests that wind observations have limited efficacy in improving the specific humidity field.

As noted, Aeolus not only improves overall forecasts over the Arctic but also improves predictions for specific days characterized by strong winds and enhanced water vapor transport, which are associated with extreme weather events. In particular, the IAOW further reveals a two to threefold increase in impact scores (ranging from 0.5 to 1.5% for strong KE500 and 0.6 to 1.2% for intense IVT) on the wind field when forecasts are conditioned on a disturbed atmosphere, as opposed to normal days. While these results are found consistently in our diagnostics, their statistical significance is marginal and, we expect, will depend strongly on the smaller scale phenomena associated with extreme wind and IVT events. We thus strongly recommend conducting longer periods of OSEs at a higher resolution or with the use of a limited area regional forecast model.

The results also provide a compelling rationale for ECCC and other modelling centres to consider the operational assimilation of Aeolus winds. In particular, results have demonstrated

enhancements in forecast skill over data-sparse regions such as the Canadian Arctic, and for forecasts of intense wind events linked to extreme weather patterns, which can have large health, societal, and economic impacts. Notably, several European weather forecast centers, including ECMWF, DWD, Météo-France, and UK Met Office, have already embraced assimilation of Aeolus (Rennie et al., 2021; Pourret et al., 2022; Kiriakidis et al., 2023). Therefore, we recommend that weather forecast centers consider assimilating global wind profile measurements from the potential Aeolus follow-on mission, Aeolus-2, scheduled for launch in 2030 (Heliere et al., 2023).

Acknowledgments

We thank Stéphane Laroche from ECCC for the Observing System Experiments, and the ECMWF for the ERA5 data. We were supported by the Canadian Space Agency's Earth System Science Data Analysis program.

Data availability

The OSEs' MSE verified against ERA5 can be downloaded from the Borealis (https://doi.org/10.5683/SP3/C0XY1B). The ERA5 data can be downloaded from the Copernicus Climate Change Service (C3S) Climate Date Store (https://doi.org/10.24381/cds.bd0915c6, Hersbach et al., 2023).

References

Augustine, J. A., & Zipser, E. J. (1987). The Use of Wind Profilers in a Mesoscale Experiment. *Bulletin of the American Meteorological Society*, *68*(1), 4-17. https://doi.org/10.1175/1520-0477(1987)068<0004:TUOWPI>2.0.CO;2

Baker, W. E., Emmitt, G. D., Robertson, F., Atlas, R. M., Molinari, J. E., Bowdle, D. A., Paegle, J., Hardesty, R. M., Menzies, R. T., Krishnamurti, T. N., Brown, R. A., Post, M. J., Anderson, J. R., Lorenc, A. C., & McElroy, J. (1995). Lidar-Measured Winds from Space: A Key Component for Weather and Climate Prediction. *Bulletin of the American Meteorological Society*, *76*(6), 869-888. https://doi.org/10.1175/1520-0477(1995)076<0869:LMWFSA>2.0.CO;2

Bass, B., Irza, J.N., Proft, J. *et al.* (2017). Fidelity of the integrated kinetic energy factor as an indicator of storm surge impacts. *Nat Hazards* **85**, 575–595. https://doi.org/10.1007/s11069-016-2587-3

Bauer, P., Magnusson, L., Thépaut, J.-N. and Hamill, T.M. (2016), Aspects of ECMWF model performance in polar areas. Q.J.R. Meteorol. Soc., 142: 583-596. https://doi.org/10.1002/qj.2449

Bormann, N., & Thépaut, J.-N. (2004). Impact of MODIS polar winds in ECMWF's 4D-VAR data assimilation system. *Monthly Weather Review*, 132, 929–940.

Bouttier, F. and Kelly, G. (2001), Observing-system experiments in the ECMWF 4D-Var data assimilation system. *Quarterly Journal of the Royal Meteorological Society*, 127: 1469-1488. https://doi.org/10.1002/qj.49712757419

Brodie, I. and Rosewell, C. (2007). Theoretical relationships between rainfall intensity and kinetic energy variants associated with stormwater particle washoff. *Journal of Hydrology*, Volume 340, Issues 1–2, 2007, Pages 40-47, ISSN 0022-1694. https://doi.org/10.1016/j.jhydrol.2007.03.019

Buehner, M., McTaggart-Cowan, R., Beaulne, A., Charette, C., Garand, L., Heilliette, S., Lapalme, E., Laroche, S., Macpherson, S. R., Morneau, J., & Zadra, A. (2015). Implementation of Deterministic Weather Forecasting Systems Based on Ensemble–Variational Data Assimilation at Environment Canada. Part I: The Global System. *Monthly Weather Review*, *143*(7), 2532-2559. https://doi.org/10.1175/MWR-D-14-00354.1

Carminati, F., A. Migliorini, S., Ingleby, B., Bell, W., Lawrence, H., Newman, S., Hocking, J., & Smith, A. (2019). Using reference radiosondes to characterise NWP model uncertainty for improved satellite calibration and validation. *Atmospheric Measurement Techniques*, *12*(1), 83-106.

Chang, J.-M., Chen, H., Jou, J.-D., Tsou, N.-C., and Lin, G.-W. (2017). Characteristics of rainfall intensity, duration, and kinetic energy for landslide triggering in Taiwan. *Engineering Geology*, Volume 231, Pages 81-87, ISSN 0013-7952. https://doi.org/10.1016/j.enggeo.2017.10.006

Chen, C.-S., Lin, Y.-L., Zeng, H.-T., Chen, C.-Y., and Liu, C.-L. (2012). Orographic effects on heavy rainfall events over northeastern Taiwan during the northeasterly monsoon season. *Atmospheric Research*, Volume 122, 2013, Pages 310-335, ISSN 0169-8095. https://doi.org/10.1016/j.atmosres.2012.10.008

Chiara, G. D., Bonavita, M., & English, S. J. (2017). Improving the Assimilation of Scatterometer Wind Observations in Global NWP. IEEE Journal of Selected Topics in Applied Earth Observations and Remote Sensing, 10(5), 2415-2423. https://doi.org/10.1109/JSTARS.2017.2691011

Chou, C.-C. & Kushner, P.J. (2023) Scale-dependent impact of *Aeolus* winds on a global forecast system. *Quarterly Journal of the Royal Meteorological Society*, 1–15. https://doi.org/10.1002/qj.4601

Chou, C.-C., Kushner, P. J., Laroche, S., Mariani, Z., Rodriguez, P., Melo, S., and Fletcher, C. G.: Validation of the Aeolus Level-2B wind product over Northern Canada and the Arctic, Atmos. Meas. Tech., 15, 4443–4461, https://doi.org/10.5194/amt-15-4443-2022

Cohen, J., Screen, J., Furtado, J. *et al.* (2014). Recent Arctic amplification and extreme mid-latitude weather. *Nature Geosci* **7**, 627–637. https://doi.org/10.1038/ngeo2234

Cordeira, J. M., & Ralph, F. M. (2021). A Summary of GFS Ensemble Integrated Water Vapor Transport Forecasts and Skill along the U.S. West Coast during Water Years 2017–20. *Weather and Forecasting*, *36*(2), 361-377. https://doi.org/10.1175/WAF-D-20-0121.1

Dai, C., Wang, Q., Kalogiros, J. A., Lenschow, D. H., Gao, Z., & Zhou, M. (2014). Determining boundary-layer height from aircraft measurements. *Boundary-layer meteorology*, *152*, 277-302.

DiMego, G. J., & Bosart, L. F. (1982). The Transformation of Tropical Storm Agnes into an Extratropical Cyclone. Part II: Moisture, Vorticity and Kinetic Energy Budgets. *Monthly*

574 *Weather Review*, *110*(5), 412-433. https://doi.org/10.1175/1520-
575 0493(1982)110<0412:TTOTSA>2.0.CO;2

576 Durre, I., Yin, X., Vose, R. S., Applequist, S., & Arnfield, J. (2018). Enhancing the Data
577 Coverage in the Integrated Global Radiosonde Archive. *Journal of Atmospheric and*
578 *Oceanic Technology*, *35*(9), 1753-1770. https://doi.org/10.1175/JTECH-D-17-0223.1

579 Eicken, H. (2013). Arctic sea ice needs better forecasts. *Nature*, *497*(7450), 431-433.

580 Eikeland, O. F., Hovem, F. D., Olsen, T. E., Chiesa, M., Bianchi. F. M. (2022). Probabilistic
581 forecasts of wind power generation in regions with complex topography using deep
582 learning methods: An Arctic case. *Energy Conversion and Management: X*, Volume 15,
583 2022, 100239, ISSN 2590-1745. https://doi.org/10.1016/j.ecmx.2022.100239

584 Francis, J.A., Vavrus, S.J. and Cohen, J. (2017), Amplified Arctic warming and mid-latitude
585 weather: new perspectives on emerging connections. *WIREs Clim Change*, 8: e474.
586 https://doi.org/10.1002/wcc.474

587 Garrett, K., Liu, H., Ide, K., Hoffman, R.N. & Lukens, K.E. (2022). Optimization and impact
588 assessment of Aeolus HLOS wind assimilation in NOAA's global forecast
589 system. *Quarterly Journal of the Royal Meteorological Society*, 148(747), 2703–2716.
590 https://doi.org/10.1002/qj.4331

591 Gascard, JC., Riemann-Campe, K., Gerdes, R. *et al.* (2017). Future sea ice conditions and
592 weather forecasts in the Arctic: Implications for Arctic shipping. *Ambio* **46** (Suppl 3),
593 355–367. https://doi.org/10.1007/s13280-017-0951-5

594 George, G., Halloran, G., Kumar, S., Rani, S. I., Bushair, M.T., Jangid, B. P., George, J. P., and
595 Maycock, A. (2021). Impact of Aeolus Horizontal Line of Sight Wind Observations in a

Global NWP System" *Atmospheric Research* 261 (October): 105742. https://doi.org/10.1016/j.atmosres.2021.105742

Gershunov, A., Shulgina, T., Ralph, F. M., Lavers, D. A., and Rutz, J. J. (2017), Assessing the climate-scale variability of atmospheric rivers affecting western North America, *Geophyical Research Letter.*, 44, 7900–7908, doi:10.1002/2017GL074175.

Graham, R.J., Anderson, S.R. and Bader, M.J. (2000), The relative utility of current observation systems to global-scale NWP forecasts. *Quarterly Journal of the Royal Meteorological Society*, 126: 2435-2460. https://doi.org/10.1002/qj.49712656805

Heliere, A., Wernham, D., Mason, G., De Villele, G., Corselle, B., Lecrenier, O., Belhadj, T., Bravetti, P., Arnaud, S., Bon, D., Lingot, P., Foulon, R., Marchais, D., Olivier, M., D'Ottavi, A., Verzegnassi, F., Mondello, A., Coppola, F., Landi, G., Hoffmann, H.-D., Esser, D., Prieto, L.P., Wührer, C., Rivers, C., Bell, R. (2023). Status of Aeolus-2 mission pre-development activities. Proc. SPIE 12777, *International Conference on Space Optics — ICSO 2022*, 1277709. https://doi.org/10.1117/12.2688794

Hersbach, H., Bell, B., Berrisford, P., Biavati, G., Horányi, A., Muñoz Sabater, J., Nicolas, J., Peubey, C., Radu, R., Rozum, I., Schepers, D., Simmons, A., Soci, C., Dee, D., Thépaut, J-N. (2023). ERA5 hourly data on pressure levels from 1940 to present. Copernicus Climate Change Service (C3S) Climate Data Store (CDS). https://doi.org/10.24381/cds.bd0915c6

Hills, R. C. (1979). The Structure of the Inter-Tropical Convergence Zone in Equatorial Africa and Its Relationship to East African Rainfall. *Transactions of the Institute of British Geographers*, *4*(3), 329–352. https://doi.org/10.2307/622055

618 Horányi, A., Cardinali, C., Rennie, M. and Isaksen, L. (2015), The assimilation of horizontal
619 line-of-sight wind information into the ECMWF data assimilation and forecasting
620 system. Part I: The assessment of wind impact. *Quarterly Journal of the Royal*
621 *Meteorological Society*, 141: 1223-1232. https://doi.org/10.1002/qj.2430

622 Inoue, J., Yamazaki, A., Ono, J., Dethloff, K., Maturilli, M., Neuber, R., ... & Yamaguchi, H.
623 (2015). Additional Arctic observations improve weather and sea-ice forecasts for the
624 Northern Sea Route. *Scientific Reports*, *5*(1), 16868.

625 James, E. P., Benjamin, S. G., & Jamison, B. D. (2020). Commercial-Aircraft-Based
626 Observations for NWP: Global Coverage, Data Impacts, and COVID-19. *Journal of*
627 *Applied Meteorology and Climatology*, *59*(11), 1809-1825.
628 https://doi.org/10.1175/JAMC-D-20-0010.1

629 Jiang, Q. (2003). Moist dynamics and orographic precipitation. *Tellus A*: Dynamic Meteorology
630 and Oceanography, 55:4, 301-316, DOI: 10.3402/tellusa.v55i4.14577

631 Joe, P., Melo, S., Burrows, W. R., Casati, B., Crawford, R. W., Deghan, A., Gascon, G., Mariani,
632 Z., Milbrandt, J., & Strawbridge, K. (2020). The Canadian Arctic Weather Science
633 Project: Introduction to the Iqaluit Site. *Bulletin of the American Meteorological*
634 *Society*, *101*(2), E109-E128. https://doi.org/10.1175/BAMS-D-18-0291.1

635 Jung, T., Kasper, M. A., Semmler, T., & Serrar, S. (2014). Arctic influence on subseasonal
636 midlatitude prediction. *Geophysical Research Letters*, *41*(10), 3676-3680.

637 Jung, T., Gordon, N. D., Bauer, P., Bromwich, D. H., Chevallier, M., Day, J. J., Dawson, J.,
638 Doblas-Reyes, F., Fairall, C., Goessling, H. F., Holland, M., Inoue, J., Iversen, T., Klebe,
639 S., Lemke, P., Losch, M., Makshtas, A., Mills, B., Nurmi, P., Perovich, D., Reid, P.,

Renfrew, I. A., Smith, G., Svensson, G., Tolstykh, M., & Yang, Q. (2016). Advancing Polar Prediction Capabilities on Daily to Seasonal Time Scales. *Bulletin of the American Meteorological Society*, *97*(9), 1631-1647. https://doi.org/10.1175/BAMS-D-14-00246.1

Kim, G., Kim, J. & Cha, DH. (2022) Added value of high-resolution regional climate model in simulating precipitation based on the changes in kinetic energy. *Geosci. Lett.* **9**, 38. https://doi.org/10.1186/s40562-022-00247-6

Kiriakidis, P., Gkikas, A., Papangelis, G., Christoudias, T., Kushta, J., Proestakis, E., Kampouri, A., Marinou, E., Drakaki, E., Benedetti, A., Rennie, M., Retscher, C., Straume, A. G., Dandocsi, A., Sciare, J., and Amiridis, V. (2023). The impact of using assimilated Aeolus wind data on regional WRF-Chem dust simulations. *Atmos. Chem. Phys.*, 23, 4391–4417. https://doi.org/10.5194/acp-23-4391-2023

Laroche, S. & Poan, E.D. (2021). Impact of the Arctic observing systems on the ECCC global weather forecasts. *Quarterly Journal of the Royal Meteorological Society*, 148(742), 252–271. https://doi.org/10.1002/qj.4203

Laroche, S. & St-James, J. (2022) Impact of the Aeolus Level-2B horizontal line-of-sight winds in the Environment and Climate Change Canada global forecast system. *Quarterly Journal of the Royal Meteorological Society*, 148(745), 2047–2062. https://doi.org/10.1002/qj.4300

Lawrence, H, Bormann, N, Sandu, I, Day, J, Farnan, J, Bauer, P. (2019). Use and impact of Arctic observations in the ECMWF Numerical Weather Prediction system. *Quarterly Journal of the Royal Meteorological Society*,145: 3432–3454. https://doi.org/10.1002/qj.3628

Lawrence, Z. D., Perlwitz, J., Butler, A. H., Manney, G. L., Newman, P. A., Lee, S. H., & Nash, E. R. (2020). The remarkably strong Arctic stratospheric polar vortex of winter 2020: Links to record-breaking Arctic Oscillation and ozone loss. *Journal of Geophysical Research: Atmospheres*, 125, e2020JD033271. https://doi.org/10.1029/2020JD033271

Le Marshall, J., Jung, J., Zapotocny, T., Redder, C., Dunn, M., Daniels, J., & Riishojgaard, L. P. (2008). Impact of MODIS atmospheric motion vectors on a global NWP system. *Australian Meteorological Magazine*, 57, 45–51.

Liu, B., Guo, J., Gong, W., Shi, L., Zhang, Y., & Ma, Y. (2020). Characteristics and performance of wind profiles as observed by the radar wind profiler network of China. *Atmospheric Measurement Techniques*, *13*(8), 4589-4600.

Martinez, C., Goddard, L., Kushnir, Y. *et al.* (2019). Seasonal climatology and dynamical mechanisms of rainfall in the Caribbean. *Clim Dyn* **53**, 825–846. https://doi.org/10.1007/s00382-019-04616-4

Martin, A., Weissmann, M., and Cress, A. (2023). Investigation of links between dynamical scenarios and particularly high impact of Aeolus on numerical weather prediction (NWP) forecasts. *Weather Climate Dynamics*, 4, 249–264. https://doi.org/10.5194/wcd-4-249-2023

Mattingly, K. S., Ramseyer, C. A., Rosen, J. J., Mote, T. L., and Muthyala, R. (2016), Increasing water vapor transport to the Greenland Ice Sheet revealed using self-organizing maps. *Geophys. Res. Lett.*, 43, 9250–9258. https://doi.org/10.1002/2016GL070424

McTaggart-Cowan, R., Vaillancourt, P. A., Zadra, A., Chamberland, S., Charron, M., Corvec, S., et al. (2019). Modernization of atmospheric physics parameterization in Canadian

NWP. *Journal of Advances in Modeling Earth Systems*, 11, 3593–3635. https://doi.org/10.1029/2019MS001781

Mile, M., Azad, R., & Marseille, G.-J. (2022). Assimilation of Aeolus Rayleigh-clear winds using a footprint operator in AROME-Arctic mesoscale model. *Geophysical Research Letters*, 49, e2021GL097615. https://doi.org/10.1029/2021GL097615

Misra, V., DiNapoli, S., & Powell, M. (2013). The Track Integrated Kinetic Energy of Atlantic Tropical Cyclones. *Monthly Weather Review*, *141*(7), 2383-2389. https://doi.org/10.1175/MWR-D-12-00349.1

Mizyak, V. G., Shlyaeva, A. V., & Tolstykh, M. A. (2016). Using satellite-derived Atmospheric Motion Vector (AMV) observations in the ensemble data assimilation system. Russian Meteorology and Hydrology, 41, 439-446. https://doi.org/10.3103/S1068373916060091

Naakka, T., Nygård, T., Tjernström, M., Vihma, T., Pirazzini, R., & Brooks, I. M. (2019). The impact of radiosounding observations on numerical weather prediction analyses in the Arctic. *Geophysical Research Letters*, 46, 8527–8535. https://doi.org/10.1029/2019GL083332

Olaguera, L.M.P., Caballar, M.E., De Mata, J.C. *et al.* (2021). Synoptic conditions and potential causes of the extreme heavy rainfall event of January 2009 over Mindanao Island, Philippines. *Nat Hazards* **109**, 2601–2620. https://doi.org/10.1007/s11069-021-04934-z

Overland, J., Francis, J. A., Hall, R., Hanna, E., Kim, S., & Vihma, T. (2015). The Melting Arctic and Midlatitude Weather Patterns: Are They Connected?. *Journal of Climate*, *28*(20), 7917-7932. https://doi.org/10.1175/JCLI-D-14-00822.1

Palmén, E. (1958), Vertical Circulation and Release of Kinetic Energy during the Development of Hurricane Hazel into an Extratropical Storm. *Tellus*, 10: 1-23. https://doi.org/10.1111/j.2153-3490.1958.tb01982.x

Pourret, V., Šavli, M., Mahfouf, J.-F., Raspaud, D., Doerenbecher, A., Bénichou, H., et al. (2022) Operational assimilation of Aeolus winds in the Météo-France global NWP model ARPEGE. *Quarterly Journal of the Royal Meteorological Society*, 148(747), 2652–2671. https://doi.org/10.1002/qj.4329

Radić, V., Cannon, A. J., Menounos, B., and Gi, N. (2015), Future changes in autumn atmospheric river events in British Columbia, Canada, as projected by CMIP5 global climate models. *J. Geophys. Res. Atmos.*, 120, 9279–9302. https://doi.org/10.1002/2015JD023279

Randriamampianina, R., Bormann, N., Køltzow, M. A., Lawrence, H., Sandu, I., & Wang, Z. Q. (2021). Relative impact of observations on a regional Arctic numerical weather prediction system. *Quarterly Journal of the Royal Meteorological Society*, *147*(737), 2212-2232.

Randriamampianina, R., Schyberg, H., & Mile, M. (2019). Observing System Experiments with an Arctic Mesoscale Numerical Weather Prediction Model. *Remote Sensing*, *11*(8), 981. https://doi.org/10.3390/rs11080981

Rani, S. I., Sharma, P., George, J. P., & Das Gupta, M. (2021). Assimilation of individual components of radiosonde winds: An investigation to assess the impact of single-component winds from space-borne measurements on NWP. *Journal of Earth System Science*, *130*(2), 89.

Rennie, M.P., Isaksen, L., Weiler, F., de Kloe, J., Kanitz, T. & Reitebuch, O. (2021). The impact of Aeolus wind retrievals on ECMWF global weather forecasts. *Quarterly Journal of the Royal Meteorological Society*, 147(740), 3555–3586. https://doi.org/10.1002/qj.4142

Reynolds, C. A., Crawford, W., Huang, A., Barton, N., Janiga, M. A., McLay, J., Flatau, M., Frolov, S., & Rowley, C. (2022). Analysis of Integrated Vapor Transport Biases. *Monthly Weather Review, 150*(5), 1097-1113. https://doi.org/10.1175/MWR-D-21-0198.1

Smith, G. C., Bélanger, J., Roy, F., Pellerin, P., Ritchie, H., Onu, K., Roch, M., Zadra, A., Colan, D. S., Winter, B., Fontecilla, J., & Deacu, D. (2018). Impact of Coupling with an Ice–Ocean Model on Global Medium-Range NWP Forecast Skill. *Monthly Weather Review*, *146*(4), 1157-1180. https://doi.org/10.1175/MWR-D-17-0157.1

Tan, X., Gan, T.Y., & Chen, Y.D. (2019). Synoptic moisture pathways associated with mean and extreme precipitation over Canada for summer and fall. *Clim Dyn* **52**, 2959–2979. https://doi.org/10.1007/s00382-018-4300-6

Velden, C. S., Hayden, C. M., Nieman, S. J., Menzel, W. P., Wanzong, S., & Goerss, J. S. (1997). Upper-tropospheric winds derived from geostationary satellite water vapor observations. *Bulletin of the American Meteorological Society*, 78, 173–195. https://doi.org/10.1175/1520-0477(1997)078,0173:UTWDFG.2.0.CO;2

Velden, C., Lewis, W. E., Bresky, W., Stettner, D., Daniels, J., & Wanzong, S. (2017). Assimilation of High-Resolution Satellite-Derived Atmospheric Motion Vectors: Impact on HWRF Forecasts of Tropical Cyclone Track and Intensity. *Monthly Weather Review*, 145, 1107-1125. https://doi.org/10.1175/MWR-D-16-0229.1

748 Young, I. R., Sanina, E., & Babanin, A. V. (2017). Calibration and Cross Validation of a Global
749 Wind and Wave Database of Altimeter, Radiometer, and Scatterometer Measurements.
750 *Journal of Atmospheric and Oceanic Technology*, 34, 1285-1306.

751 Zuo, H. and Hasager, C. B. (2023). The impact of Aeolus winds on near-surface wind forecasts
752 over tropical ocean and high-latitude regions. *Atmospheric Measurement Technique*, 16,
753 3901-3913. https://doi.org/10.5194/amt-16-3901-2023

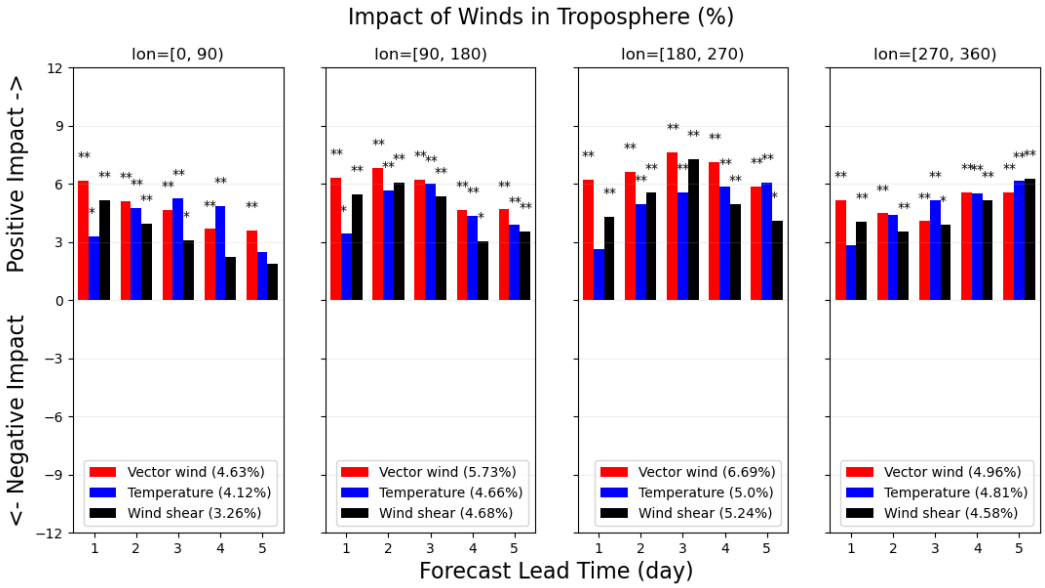

SFigure 1: Similar to Figure 1(a), but for the impact score over subregions over the Arctic.

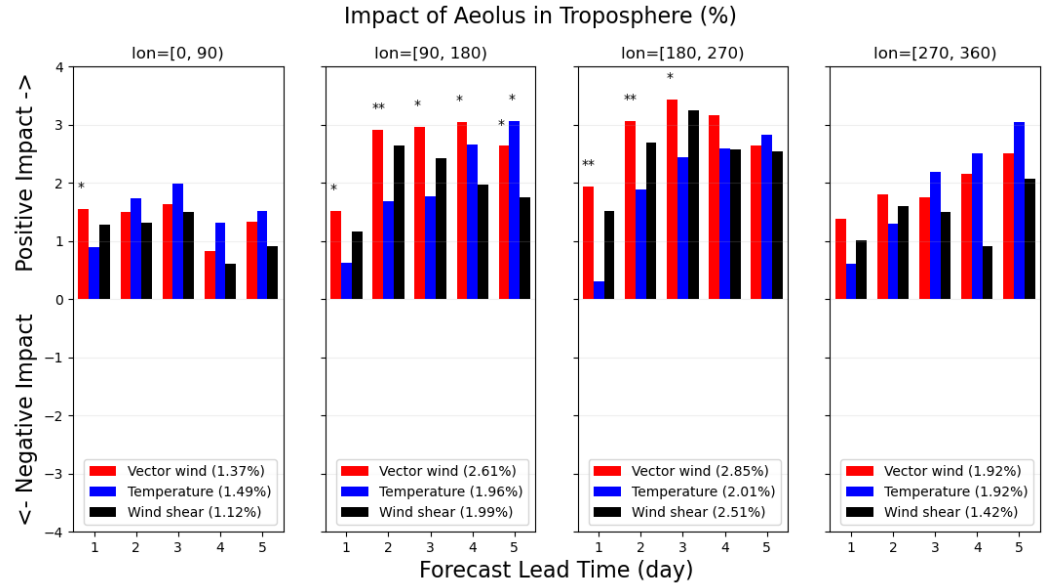

SFigure 2: Similar to Figure 1(b), but for the impact score over subregions over the Arctic.

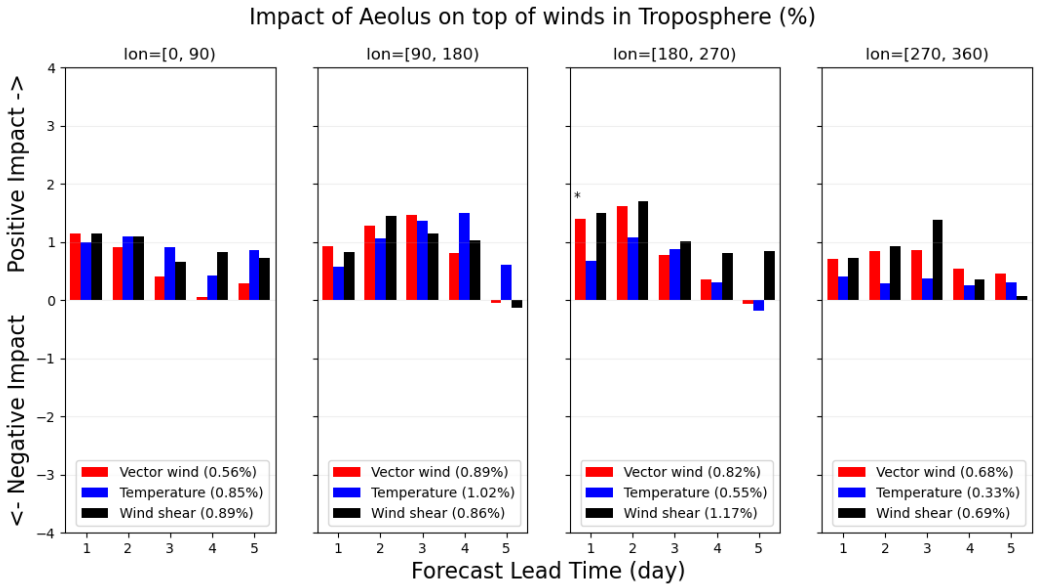

SFigure 3: Similar to Figure 1(c), but for the impact score over subregions over the Arctic.

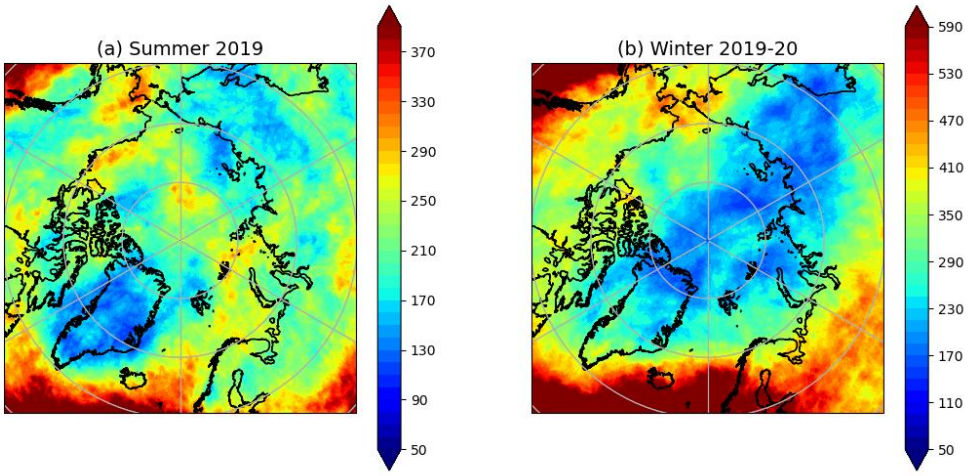

SFigure 4: An Arctic view of the 90th percentile of the 500-hPa Kinetic Energy (KE500, in m^2/s^2) from ERA5 during (a) Summer 2019 and (b) Winter 2019-20.

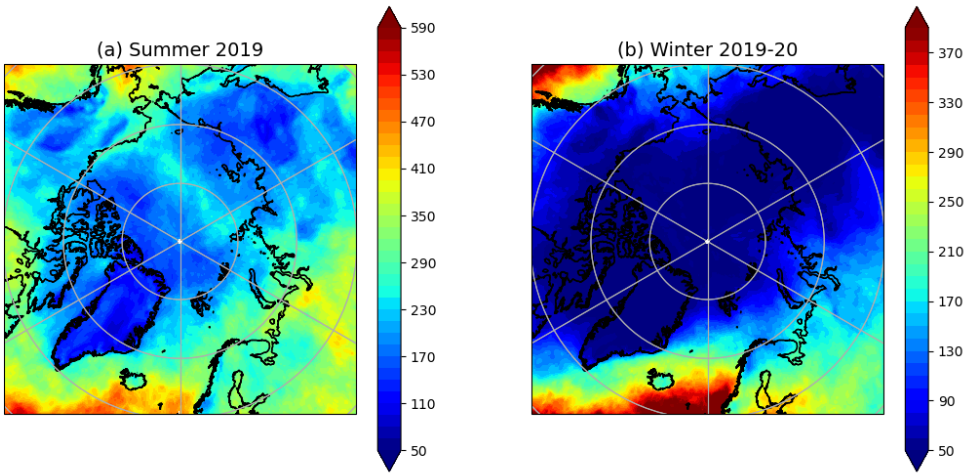

SFigure 5: Similar to SFigure 4, but for the 90th percentile of the integrated vapor transport (IVT, in $kg/m \cdot s$).

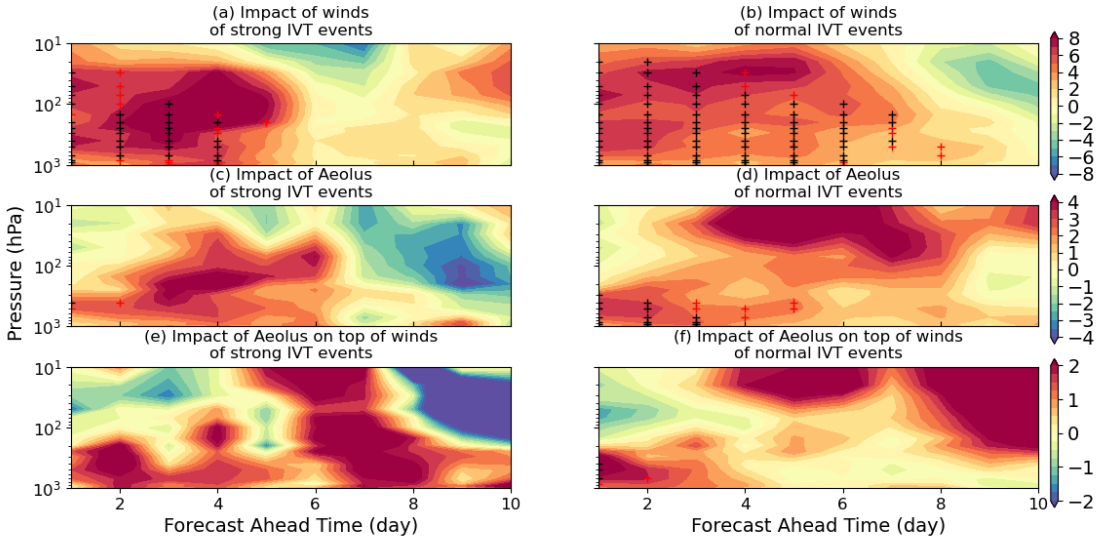

SFigure 6: Similar to Figure 7, but for impacts of the added wind observations of strong IVT days and normal IVT days.